JPn Neuroscience
The Journal of Physiology

Accumulation of K^+ in the synaptic cleft modulates activity by influencing both vestibular hair cell and calyx afferent in the turtle

Donatella Contini, Steven D. Price and Jonathan J. Art

Department of Anatomy and Cell Biology, College of Medicine, University of Illinois at Chicago, Chicago, IL 60612, USA

Key points

- In the synaptic cleft between type I hair cells and calyceal afferents, K^+ ions accumulate as a function of activity, dynamically altering the driving force and permeation through ion channels facing the synaptic cleft.
- High-fidelity synaptic transmission is possible due to large conductances that minimize hair cell and afferent time constants in the presence of significant membrane capacitance.
- Elevated potassium maintains hair cells near a potential where transduction currents are sufficient to depolarize them to voltages necessary for calcium influx and synaptic vesicle fusion.
- Elevated potassium depolarizes the postsynaptic afferent by altering ion permeation through hyperpolarization-activated cyclic nucleotide-gated (HCN) channels, and contributes to depolarizing the afferent to potentials where a single EPSP (quantum) can generate an action potential.
- With increased stimulation, hair cell depolarization increases the frequency of quanta released, elevates $[K^+]_{cleft}$ and depolarizes the afferent to potentials at which smaller and smaller EPSPs would be sufficient to trigger APs.

Abstract Fast neurotransmitters act in conjunction with slower modulatory effectors that accumulate in restricted synaptic spaces found at giant synapses such as the calyceal endings in the auditory and vestibular systems. Here, we used dual patch-clamp recordings from turtle vestibular hair cells and their afferent neurons to show that potassium ions accumulating in the synaptic cleft modulated membrane potentials and extended the range of information transfer. High-fidelity synaptic transmission was possible due to large conductances that minimized hair cell and afferent time constants in the presence of significant membrane capacitance. Increased potassium concentration in the cleft maintained the hair cell near potentials that promoted the influx of calcium necessary for synaptic vesicle fusion. The elevated potassium concentration also depolarized the postsynaptic neuron by altering ion permeation through hyperpolarization-activated cyclic nucleotide-gated (HCN) channels. This depolarization enabled the afferent to reliably generate action potentials evoked by single AMPA-dependent EPSPs. Depolarization of the postsynaptic afferent could also elevate potassium in the synaptic cleft, and would depolarize other hair cells enveloped by the same neuritic process increasing the fidelity of neurotransmission at those synapses as well. Collectively, these data demonstrate that neuronal activity gives rise to potassium accumulation, and suggest that potassium ion action on HCN channels can modulate neurotransmission, preserving the fidelity of high-speed synaptic transmission by dynamically shifting the resting potentials of both presynaptic and postsynaptic cells.

(Received 5 July 2016; accepted after revision 11 September 2016; first published online 16 September 2016)
Corresponding author J. J. Art: Department of Anatomy and Cell Biology, College of Medicine, University of Illinois at Chicago, Chicago, IL 60612, USA. Email: jart@uic.edu

DOI: 10.1113/JP273060

Abbreviations 4-AP, 4-aminopyridine; AMPAR, AMPA receptor; AP, action potential; ASIC, acid-sensing ion channel; BK, large calcium-activated potassium channel; CNQX, 6-cyano-7-nitroquinoxaline-2,3-dione; CV, coefficient of variation; CV*, normalized coefficient of variation; DAPI, 4′,6-diamidino-2-phenylindole; EPSC, excitatory postsynaptic current; EPSP, excitatory postsynaptic potential; HCN, hyperpolarization-activated cyclic nucleotide-gated channel; I_{Ca}, calcium current; I_h, hyperpolarization-activated current; I_K, potassium current; IK_{Ca}, calcium-activated potassium current; IK_{LV}, low-voltage-activated potassium current; rms, root mean square; TEA, tetraethylammonium; ZD7288, 4-ethylphenylamino-1,2-dimethyl-6-methylaminopyrimidinium chloride.

Introduction

Fast synaptic transmission modulated by the co-release of other effectors is a common motif in the nervous system (Vaaga *et al.* 2014). At some synapses, the close and extensive apposition of the presynaptic and postsynaptic neurons may increase the complexity of interaction by limiting diffusion (Wersäll, 1956; Schneggenburger & Forsythe, 2006; Borst & Soria van Hoeve, 2012). At others, astrocytes may impose similar barriers (Araque *et al.* 1999), and create delimited volumes into which they too may release active compounds that influence transmission between the presynaptic and postsynaptic neurons (Nedergaard, 1994; Parpura *et al.* 1994; Haydon & Nedergaard, 2015). In both cases, ions flowing from either cell can dynamically alter ion concentrations in the synaptic cleft, and change the permeability and driving force for currents through presynaptic and postsynaptic channels. This will have a significant impact on the membrane potential of both cells, and may also influence the speed and fidelity with which high-frequency information is transmitted across the synapse (Leao *et al.* 2011).

The notion that local ion accumulation can modulate neuronal activity has long been recognized (Frankenhaeuser & Hodgkin, 1956). For example, the restricted space created by glia surrounding the squid axon results in dynamic changes in $[K^+]_o$ following activity (Adelman *et al.* 1973). This local concentration differs significantly from that in the bath, and alters the potassium equilibrium potential. The action of $[K^+]_o$ as a modulator during activity has also been demonstrated for skeletal muscle (Almers, 1972), and cardiac Purkinje fibres (Cohen *et al.* 1976). A theoretical analysis predicted that this would be a general phenomenon in restricted spaces around all excitable cells (Attwell & Iles, 1979). Recordings from the dorsal root (Nicoll, 1979), and neuromuscular junction (Katz & Miledi, 1982) revealed discernible effects due to the accumulation of K^+ during activity or synaptic transmission. Possible modulation due to changes in $[H^+]_o$ is of interest as well since H^+ activation of proton receptors was discovered in sensory neurons (Krishtal & Pidoplichko, 1981*a*,*b*). In addition, the subsequent demonstration that $[H^+]_o$ modulated Ca^{2+} permeation necessary for synaptic transmission in photoreceptors (DeVries, 2001) and hair cells (Cho & von Gersdorff, 2014) led to the conclusion that dynamic changes in $[H^+]_o$ could affect synaptic transmission by two distinct routes.

In principle, the effects of changes in ion concentration should be a factor for all neurons, and be even more dramatic on transmission at small central synapses. Indeed, the effects of pH on synaptic plasticity via an acid sensing ion channel (ASIC) have been examined experimentally (Du *et al.* 2014; Kreple *et al.* 2014). By contrast, an equivalent analysis of the role played by K^+ modulation on excitability has been largely theoretical (Attwell *et al.* 1979; Chen, 1995; Goldberg, 1996*a*,*b*), and little is known about how the dynamic changes in K^+ concentration influence neuronal synaptic function in the CNS. The femtolitre volume and the challenge of controlling the membrane potential in both the presynaptic and postsynaptic neurons make it remarkably difficult to measure and analyse the functional significance of changes in ion concentration at any synapse. The effects of these changes have been investigated previously in giant synapses in the vestibular system using ion-sensitive optical indicators for H^+ dynamics (Highstein *et al.* 2014), and with recordings from either the presynaptic hair cell or the postsynaptic afferent neuron (Contini, 2011; Lim *et al.* 2011; Contini *et al.* 2012; Highstein *et al.* 2014). However, understanding the functional significance of the changes in concentration of H^+, K^+, or any other ion on synaptic transmission requires knowledge of the simultaneous effects of the concentration changes on both the presynaptic and the postsynaptic cells.

Using vestibular hair cells as a model system, we have made the first paired recordings from hair cells and their enveloping afferent neurons to analyse changes in potassium concentration in the cleft. We find that K^+ accumulation changes the K^+ equilibrium potential, and significantly contributes to depolarizing the hair cell to voltages that activate the calcium current necessary for synaptic transmission. Further, we show that an elevated synaptic K^+ concentration generates an inward current through HCN channels in the postsynaptic afferent that shifts the membrane potential toward the threshold for action potential generation. As a result, the elevated synaptic $[K^+]_o$ enables a single vesicle (quantum) released presynaptically to trigger a single action potential in the postsynaptic afferent. This would ensure that the statistics of postsynaptic activity match the statistics of vesicle release, thereby maintaining high-frequency, high-fidelity

information transfer. We also found that depolarization of the afferent in turn would increase $[K^+]_o$ at neighbouring synapses and depolarize other hair cells enveloped by the same afferent. In aggregate these results suggest that K^+ accumulation at synapses following elevated activity may serve as a slow neuromodulator of faster synaptic events, and roles traditionally characterized as presynaptic and postsynaptic are complicated by their interaction in a restricted volume.

Methods

Ethical approval

Experiments used tissue harvested from red-eared turtles, *Trachemys scripta elegans*, housed in the Association for the Assessment and Accreditation of Laboratory Animal Care accredited UIC Biologic Resource Laboratory. Experimental protocol 13-032 was approved by the University of Illinois at Chicago Institutional Animal Care and Use Committee, according to National Institutes of Health guidelines (assurance number A3460-01). Turtles were killed and decapitated following I.M. injection of ketamine, 6 mg kg^{-1}, according to the American Veterinary Medical Association guidelines.

Epithelia isolation

All experiments were performed on isolated vestibular epithelia from the posterior semicircular canal of turtles of either sex (carapace 10–15 cm, 90–140 g, $n = 226$, 90 males, 136 females). Following decapitation, the head was split in the mid-sagittal plane and immersed in a 4°C, oxygenated low-Ca^{2+} Ringer solution containing (in mM): 121 NaCl, 4 KCl, 0.45 $CaCl_2$, 2.2 $MgCl_2$, 10 Na-Hepes, 2 sodium pyruvate, 2 creatine monohydrate, at pH 7.6. All reagents were from Sigma-Aldrich (St Louis, MO, USA). The brain was partially removed, leaving the brainstem between the cerebellar angle and glossopharyngeal nerve (CNIX) attached to the statoacoustic nerve (CNVIII). The medial, cartilaginous aspect of the temporal bone was reflected, and the posterior canal, basilar papilla and a portion of the saccule were isolated *en bloc*. The posterior canal and its associated branch of nerve and brainstem were isolated and transferred in a fluid-filled Silanized Pasteur pipette to the recording chamber. Modifying the technique of Chatlani (2011), the vault of the posterior canal was opened with iris scissors to expose the crista. The canal and epithelium were then oriented so that the mechanically sensitive ciliary bundles were in the horizontal plane (Fig. 1*D*), and were pinned to Parafilm that was heat-sealed to the glass bottom of the chamber. To visualize the hair cells and enveloping afferent terminals from an exposed lateral aspect, the epithelium was bisected along the ridge of the crista normal to the axis of the canal, the supporting cell layer and connective tissue undercut, and the upper side of the epithelium removed with fine tweezers.

Microscopic visualization and reconstruction

The 320 μl Perspex experimental chamber was mounted on a fixed-stage, upright Zeiss Axioskop FS-II microscope and perfused at 1 ml min^{-1} with 24–27°C oxygenated artificial perilymph (in mM): 121 NaCl, 4 KCl, 2.8 $CaCl_2$, 2.2 $MgCl_2$, 10 Na-Hepes, 2 sodium pyruvate, 2 creatine monohydrate, at pH 7.6, using a custom constant-velocity peristaltic pump and controller. The preparation was visualized using a 40×, 0.8 NA, 3.6 mm working distance water immersion objective, with additional 2× optovar magnification. Both video low-light differential interference contrast (DIC) and widefield fluorescence images were captured using an $iXon_3$ 897, EMCCD camera, QE > 90% (Andor Technology, Belfast, UK). For subsequent confocal images, the cristae were fixed in paraformaldehyde and washed three times in 0.1 M phosphate buffer, trimmed of their excess nerve and connective tissue, and mounted in Mowiol containing DAPI (EMD Millipore, Temecula, CA, USA) onto 10 well slides (Erie Scientific, Portsmouth, NH, USA). The tissue was examined and image stacks obtained using a ZEISS LSM 710 confocal microscope, and reconstructed using ZEN software (Zeiss, Thornwood, NY, USA).

Electrophysiology

Except where otherwise noted, dual-electrode recordings were made with borosilicate electrodes filled with (in mM): 118 KF, 12 KCl, 5 K_2-EGTA, 5.45 K-Hepes, 5 Na_2ATP, 175 μM Li_2-GTP, at pH 7.2. The solution for hair cells contained 50 μM Alexa Fluor 488, and that for the afferents, 50 μM Alexa Fluor 568 (Invitrogen, Carlsbad, CA, USA), to facilitate morphological reconstruction. Pharmacological blockers 6-cyano-7-nitroquinoxaline-2,3-dione (CNQX), tetrodotoxin (TTX), and 4-ethylphenylamino-1,2-dimethyl-6-methylaminopyrimidinium chloride (ZD7288) were from Tocris (Bio-Techne, Minneapolis, MN, USA). Simultaneous presynaptic and postsynaptic recordings were made with a MultiClamp 700B amplifier (Molecular Devices, Sunnyvale, CA, USA). Electrode capacitance and liquid junction potentials (average –53 mV) were offset just prior to sealing onto the cells.

Recording electrodes had initial series resistances in the bath of 3–5 MΩ, and final resistances upon achieving whole-cell configuration of ~3× their initial values. The amplifier compensation circuit was used to compensate up to 65% of the access resistance, when the compensatory feedback was low-pass filtered at 4.5–5.0 kHz. This resulted in final access resistances close to the initial values measured in the bath. We used the capacity transients at

the beginning and the end of small, 5–10 mV, commands at the holding potentials to estimate the access resistance, membrane resistance and whole-cell capacitance of both cells. The transients were converted with 50 MΩ feedback resistors, filtered at 20 kHz and digitized at 200 kHz.

Since the capacity transient was used to monitor changes in access resistance continuously during the experiments, only the R_s 'compensation' circuit was used (max compensation typically ~60%). Predictive compensation was not used since it neither improved the dynamic response of the clamp nor corrected for voltage errors due to current flow across the access resistance (Molecular Devices, 2008). The access resistance, R_a, was determined from the current to charge

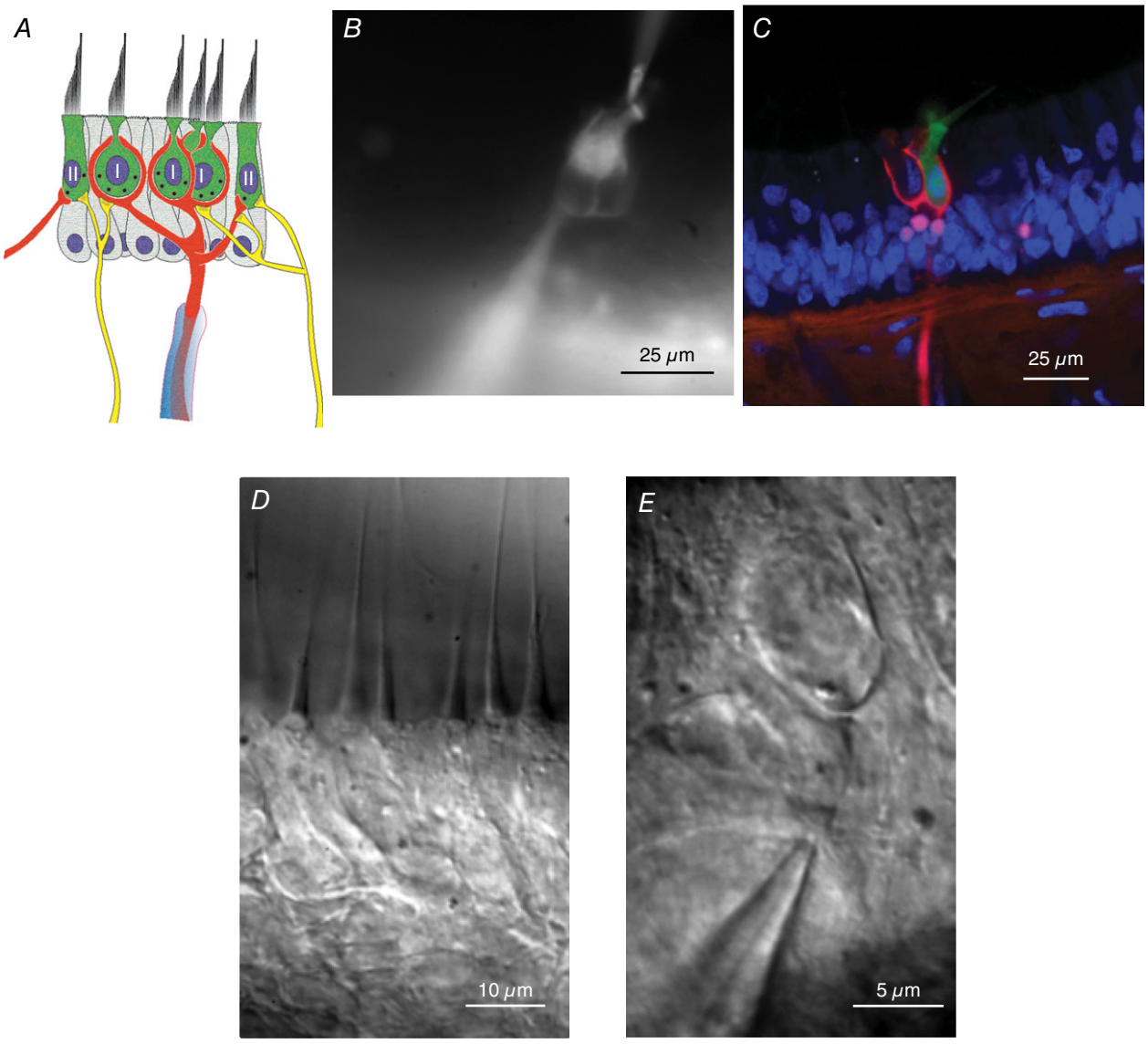

Figure 1. Dual recording from the sensory epithelium
A, schematic diagram of a primary afferent and its associated hair cells. A single myelinated afferent (red) may branch to several enveloping endings, each containing multiple type I hair cells. Additional input from type II hair cells may occur via synaptic input onto the outer face of the afferent (left-hand synapse), or through bouton endings of fine collateral branches (right-hand side). Efferent fibres (yellow) from the CNS are shown synapsing on both hair cells and the outer face of the calyx. *B*, fluorescence image of dye-filled hair cell and afferent. *C*, confocal image showing one of three hair cells (green), enveloped by a complex calyx (red), with DAPI-stained nuclei (blue). Four bouton endings associated with the dimorphic afferent are also visible (pink). *D*, central region of the posterior canal epithelium viewed in Nomarski differential interference contrast (DIC). The apical mechanically sensitive bundle is oriented toward the top of the panel, with the basolateral surface enveloped by the afferent ending below. *E*, DIC image of afferent electrode sealed onto the confluence of the afferent branches. Hair cell electrodes were sealed onto the most apical region of the basolateral surface not covered by the afferent (Fig. 1*B*).

the membrane and the time constant, τ, of the current relaxation to I_∞, where $\tau = C_m R_{(Ra \,||\, Rm)}$. The charge added to the membrane, Q_m, is the difference between the integral under the total current and the integral of current flow through the membrane resistance, R_m. For a given command, V_c, the steady-state voltage across the membrane is given by: $V_m = V_c R_m/(R_a + R_m)$. Using $\tau = (Q_m/V_m)(R_a R_m)/(R_a + R_m)$, and substituting for V_m, $R_a = \tau V_c/Q_m$. Since the total resistance, R_T, is given by: $R_T = V_c/I_\infty$, and therefore $R_m = V_c/I_\infty - R_a$.

Though stimuli are given as command voltages or currents, all figures derived from current measurements – current, conductance and reversal potential – *versus* voltage have been corrected for voltage drops due to current flow across uncompensated access resistances. Whole-cell currents were typically converted using a 50 MΩ feedback resistor for the hair cell, and 500 MΩ resistor for the afferent fibre. Currents and voltages were low-pass filtered at 10 or 2 kHz using four-pole Bessel filters, and digitized at 20 kHz. All digitization, as well as all commands for voltage and current, were under the control of a Digidata 1440A interface (Molecular Devices).

Drug perfusion

Rapid, local solution exchange was achieved by positioning the output of a Teflon MPP6 manifold (Warner Instruments, Hamden, CT, USA) within 100 μm of the cell pair. Barrels of the manifold were supplied by a Rainin Rabbit peristaltic pump (Gilson, Middleton, WI, USA), with the solution of choice directed to the manifold using a remote-controlled miniature solenoid valve (The Lee Co., Westbrook, CT, USA). Initial effects of perfusion could be recorded within 6 s of the onset of superfusion, and efficient washout was assured by having normal perilymph in at least one of the manifold barrels, in addition to the bulk bath perfusion.

Statistics

Online stimulus protocols and digitization were generated using pCLAMP 10 software (Molecular Devices). Data were imported using IGOR-compatible routines from NeuroMatic (www.neuromatic.thinkrandom.com). Offline signal processing, analysis, and figure creation used IGOR V6.35 (Wavemetrics, Portland, OR, USA).

The statistics of current and voltage records were calculated in the usual way for equally spaced data: average of all Y_i values, a; standard deviation of n values, $\sigma = \sqrt{1/(n-1)\sum (Y_i - a)^2}$; root mean square of Y_i, $\text{rms} = \sqrt{(\frac{1}{n})Y_i^2}$.

Non-linear fits to all functions were solved by an iterative least-squares method modelled on the code in *Numerical Recipes in C* (Press *et al.* 1992). Current waveforms of exponential growth or decay were fit with exponentials or double exponentials with offset, $y_0 + A e^{(t-t_0)/\tau}$, $y_0 + A_1 e^{(t-t_0)/\tau_1} + A_2 e^{(t-t_0)/\tau_2}$, where y_0 was the minimum value, A_1 and A_2 were amplitudes, and τ_1 and τ_2 were time constants. The conductance *vs.* voltage curves were fit with a sigmoidal function, $g(V) = g_0 + (\frac{g_\infty}{(1+e^{-\frac{(V-V_{0.5})}{k}})})$, where the free parameters, g_0 and g_∞, are the limiting conductances, $V_{0.5}$ the voltage of half activation, and k is a constant.

Analysis of quantal events followed prior techniques (Chatlani, 2011). Timing and amplitude of excitatory postsynaptic currents (EPSCs) and excitatory postsynaptic potentials (EPSPs) were extracted by initially segmenting the records, removing drift in the segments by fitting with a polynomial of 9th order or less, and subtracting the polynomial from the original segments. An event threshold was set at five times the root mean square of the baseline noise in portions of the record without events. Timing of events was determined by threshold crossing. An optimal (Wiener) filter, $\Phi(f)$, in the frequency domain (Press *et al.* 1992) is given by: $\Phi(f) = |S(f)|^2 / (|S(f)|^2 + |N(f)|^2)$, where S is the signal and N is the noise in the trace. The power spectrum of the original record, $S(f) + N(f)$, is the sum of the power of the signal, $S(f)$, and the power of the baseline noise, $N(f)$, obtained after events have been removed. Subtracting the power spectrum of the noise from the total power spectrum yields the power spectrum of the signal. The derived filter was applied to the original records to extract event amplitudes. Event amplitude histograms were created by binning the amplitudes of the baseline and the EPSCs or EPSPs. Integration of the amplitude histograms yielded the cumulative amplitude distributions. The coefficient of variation (CV) of inter-event intervals was determined at a given mean interval, $\bar{t}_{int}$, by dividing the standard deviation of the intervals, σ_{int}, by the mean: $\text{CV} = \frac{\sigma_{int}}{\bar{t}_{int}}$. For steady-state or ramp data, intervals were acquired over samples of 20–100 s. To remove the rate dependence of CV, a standard coefficient of variation (CV^*) at 50 ms was calculated for each cell by fitting the CV *vs.* $\bar{t}_{int}$ with a power function, $\text{CV}(\bar{t}) = K_0 + K_1(\bar{t})\text{CV}^* k_2 \bar{t}$, where K_0, K_1 and K_2 are constants.

Results

Recording from hair cells and afferent neurons

The majority of our recordings were from the central region of the turtle posterior canal epithelium, a region populated by either complex calyces, in which an afferent neuron envelops more than one hair cell (Fernandez *et al.* 1988; Brichta & Goldberg, 2000*a*), or dimorphic endings, as originally defined in lizard (Schessel & Highstein, 1981), where the afferent neuron also has branches ending in conventional boutons. The potentially complex structure

of the afferent neuron is shown schematically in Fig. 1*A*, where a pair of complex calyces join an additional thin branch to a bouton ending. Hair cells enveloped by the afferent are defined as type I hair cells, and those synapsing on the outer face of the calyx (Fig. 1*A*, left), or onto bouton endings (Fig. 1*A*, right) are defined as type II hair cells. Recordings from hair cell and afferent neuron were made with dye-filled pipettes (Fig. 1*B*). Reconstruction of confocal stacks counterstained with the nuclear stain DAPI (Fig. 1*C*) determined whether or not a hair cell was enveloped by the corresponding afferent neuron, and therefore whether it was classified as type I or type II. This also permitted a count of the number of hair cells within the afferent neuron, and an estimate of the number of bouton endings that contribute to the afferent. Dissector method estimates (Sterio, 1984) of synaptic profiles for this epithelium yielded on average 32.6 synapses between each enveloped hair cell and the inner face of its afferent neuron, and 5.7 synapses between hair cells and the outer face (Fig. 1*A*, left) (Holt *et al.* 2007). Typically, complex calyces may envelop up to five hair cells, and up to three such calyces have been observed to share a common afferent stalk. The number of additional bouton endings on a single dimorphic afferent is highly variable (Lysakowski & Goldberg, 2004). Recordings were made deep to an exposed face created by splitting the saddle-shaped epithelium (see Methods). Recording directly from the apical surface of hair cells was precluded by their small size dominated by the presence of a mechanically sensitive ciliary bundle, and the cuticular plate, an underlying actin gel into which the bundle inserts (Fig. 1*D*) (DeRosier & Tilney, 1989). Consequently, hair cells were patched on the most apical portion of the baso-lateral surface (Fig. 1*B*), a region not enveloped by the postsynaptic afferent neuron. Recordings of the afferent were made at the confluence of its branches (Fig. 1*E*).

Examination of feedforward and feedback between presynaptic type I hair cell and postsynaptic afferent

To examine modulation of presynaptic and postsynaptic potentials, we made simultaneous recordings from hair cells and their afferent neurons. In the hair cell, current injection through the recording electrode was used to mimic transduction currents (Fettiplace & Crawford, 1978). The hair cell recording in Fig. 2*A* was from one of three type I hair cells enveloped by a dimorphic afferent neuron with five additional boutons endings. Current pulses depolarized the cell from a zero current potential of –70 mV (Fig. 2*A*, upper traces). Our results differed in only one respect from previous studies of solitary semicircular canal hair cells. In isolated cells, damped oscillations in membrane potential were observed only in type II hair cells (Rennie & Ashmore, 1991). Our observation, similar to that seen in the rat saccule (Eatock & Songer, 2011), is that in their native context, type I hair cells enveloped by an afferent display critical damping, or adaptation in membrane potential. There were two components in the afferent response. The first was a slow depolarization of the afferent elicited by depolarizing the hair cell. Depolarization of the hair cell to –68.3 mV in the steady state produced a 206 μV depolarization in the afferent (light blue trace). Injection of larger currents in the hair cell generated larger depolarizations. In the hair cell, the largest depolarization to –22.1 mV (largest green trace), followed by a relaxation to –51.1 mV (–54.5 $\pm$ 3.4 mV, $n = 3$) (Fig. 2*A*, upper traces), was associated with an afferent depolarization of 5.3 mV (3.3 $\pm$ 2.1 mV) (Fig. 2*A*, lower traces). Across the population, and within hair cell–afferent pairs, the degree of hair cell and afferent depolarization was correlated. In addition, for the pair illustrated, a second component in the response was apparent when the afferent was depolarized above –74.3 mV. A series of rapid potentials, irregularly spaced but with a uniform amplitude of 3.6 mV, were superimposed on the slow depolarization. Smaller, 700 μV potentials, phase-locked to the afferent potentials, were observable in the hair cell recording (Fig. 2*A*, inset) as well for the corresponding voltages above –56.6 mV (Fig. 2*A*, upper traces). Both presynaptic and postsynaptic potentials were TTX-blockable, and as previously suggested (Chatlani, 2011), they are likely to represent action potential (AP) generation proximal to the recording site from a spike initiation zone. Their block by 300 nM TTX is consistent with the pharmacological sensitivity of $Na_V1.6$ and $Na_V1.5$ channels described in vestibular afferents (Lysakowski *et al.* 2011; Liu *et al.* 2016).

The notion that the first component of the afferent response, the slow depolarization, was in response to a slowly activating net inward current was confirmed by voltage clamping the afferent (Fig. 2*B*). In contrast to the rapid hair cell depolarizations ($\tau = 3.65 \pm 2.64$ ms, $n = 6$), the corresponding inward currents in the afferent developed with time constants 17 times longer (τ = 61.6 $\pm$ 26.1 ms). To examine this effect further, both cells were voltage clamped at –70 mV, a value typical of the resting potential of hair cells (Contini, 2011; Contini *et al.* 2012) and calyx afferents (Chatlani, 2011; Contini *et al.* 2012) in similar or more intact preparations (Holt *et al.* 2007). Of the multiple potassium conductances expressed in hair cells (Meredith & Rennie, 2016), a signature feature of those enveloped by an afferent neuron is the dominance by a low-voltage-activated conductance (IK_{LV}) (Chen, 1995; Rusch *et al.* 1998). In extracellular solutions with $[K^+]_o$ between 4 and 6 mM, IK_{LV} typically activated when depolarized above –90 mV, and was half-activated between –70 and –60 mV. As a consequence, with depolarization the hair cell current reached 90% of the steady-state value within 0.67 ms (1.22 $\pm$ 1.51 ms,

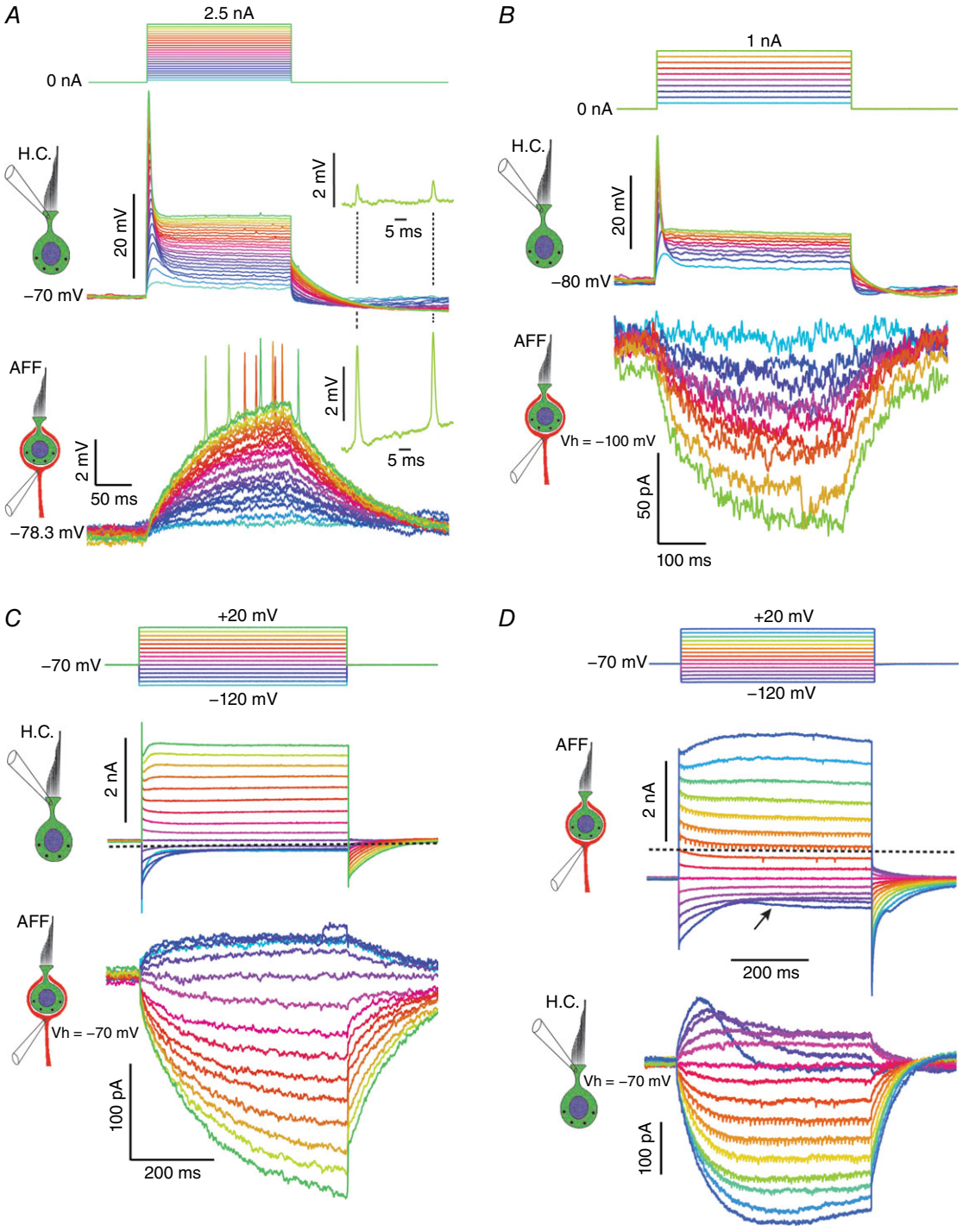

Figure 2. Paired responses of hair cell and afferent in current and voltage clamp
A, depolarizing current pulses, injected into a hair cell from the zero-current potential of –70 mV, elicit a phasic voltage response. Simultaneous current-clamp recording from the associated afferent reveal slow depolarizations that are proportional to the depolarization in the hair cell. Rapid depolarizations are visible in the largest traces when the afferent is depolarized above –74.3 mV. Synchrony of rapid afferent depolarizations and those in the hair cell for one level shown as inset. *B*, with the hair cell in current clamp and the afferent in voltage clamp, the depolarization of the hair cell (upper traces) is correlated with inward currents in the afferent (lower traces). *C*, hair cell and afferent in voltage clamp. Dashed line at zero current level. An outward current in the hair cell generates a slower inward current in the afferent, and hyperpolarization of the hair cell results in an outward current. *D*, depolarization of the afferent generates inward current in the hair cell and hyperpolarization of the afferent generates outward currents in the hair cell. Dashed line at zero current level.

$n = 15$) (Fig. 2*C*, upper traces). Progressively larger inward currents in the afferent (Fig. 2*C*, lower traces) were associated with hair cell depolarization. The increase in these currents was dominated by a single exponential, with time constants ranging from 108.2 ± 79.8 for the smallest to 83.7 ± 51.1 ms ($n = 15$) for the largest currents. Since much of the basolateral surface of the hair cell is enveloped by the afferent calyx, thereby limiting diffusion into the bath, we would expect the contents of synaptic vesicles, such as glutamate (Forsythe, 1994) and H^+ (Stadler & Tsukita, 1984), as well as K^+ (Contini, 2011; Lim *et al.* 2011) to be elevated in the synaptic cleft. As with prior analysis (Frankenhaeuser & Hodgkin, 1956; Adelman *et al.* 1973), the trajectory of the current in the afferent was well modelled as a leaky-integrator, with an exponential rise to its steady state. Such a result is consistent with the afferent current developing in proportion to the accumulation of any of the vesicular contents or ion species. Similarly, with hair cell hyperpolarization conductances that were on at rest were deactivated (Fig. 2*C*, upper traces), and at –120 mV the residual conductance of < 1 nS in the steady state was a leak to 0 mV, representing either the hair cell transducer (Ohmori, 1985) or the seal conductance. Under these conditions, we expect little Ca^{2+} flux into the hair cell, and that both vesicle fusion and potassium efflux into the cleft will be blocked. The resulting small outward current that develops in the afferent is consistent with a reduction in transmitter released, or a depression of $[\text{ions}]_{\text{cleft}}$, causing a change in the equilibrium potential or permeation for afferent conductances facing the synaptic cleft (Fig. 2*C*, lower traces).

To begin to differentiate between effects due to the release of transmitter from the hair cell and ion accumulation that might occur regardless of presynaptic or postsynaptic source, we depolarized the afferent while holding the hair cell at –70 mV. Large outward currents developed from the afferent (Fig. 2*D* upper traces), rapidly reaching 90% of the steady state (0.381 ± 0.382 ms, $n = 4$), a result consistent with previous reports (Rennie & Streeter, 2006; Dhawan *et al.* 2010; Chatlani, 2011; Meredith *et al.* 2012) that calyceal afferents have a large resting conductance. With larger depolarization, small rapid TTX-blockable transient inward currents were visible, consistent with the pharmacology of the rapid, depolarizing potentials seen in current clamp (Fig. 2*A*, lower traces). This implied a limited space clamp, with the downstream spike initiation zone not under voltage clamp. Since the afferent has significant conductances on both the inner surface delimiting the cleft and on the outer surface facing the bath (Lysakowski *et al.* 2011), an unknown fraction of the current will be flowing into the cleft. However, there was an inward current in the hair cell that was associated with depolarization and the outward current from the afferent (Fig. 2*D* lower traces). The initial phase of the hair cell current could be well fit by an exponential (53.9 ± 20.2 ms, $n = 3$) for the largest inward currents. This result would obtain if hair cell conductances or the equilibrium potential for these conductances was sensitive to transmitter or ion concentrations in the cleft, and depolarization of the afferent modulated these or changed their rates of removal from the cleft.

The time course of afferent response to hyperpolarizing steps (Fig. 2*D* upper traces) was more complex, with two distinct phases for the three most hyperpolarized steps. In the initial phase, much of the current on at –70 mV deactivated, similar to prior observations in this preparation (Chatlani, 2011). Associated with this initial inward current at –120 mV, was the onset of a net outward current in the hair cell (Fig. 2*D* lower traces. During the second phase of the response, a slow inward current developed in the afferent for hyperpolarizing steps between –90 and –120 mV (Fig. 2*D* upper traces). The pharmacological block of this current by 200 μM ZD7288 (see Fig. 7*C*), its activation at hyperpolarized potentials and its time course were all consistent with the I_h previously described in vestibular afferents and ganglion cells (Meredith *et al.* 2012; Horwitz *et al.* 2014). During this second phase, as the inward current at –120 mV increased, the net outward current in the hair cell diminished back to the resting value. For smaller afferent hyperpolarizations, the biphasic hair cell response was less prominent, and the hair cell current was well fit by an exponential. As with the response to afferent depolarization, the hair cell outward currents would develop if afferent hyperpolarization systematically decreased the concentration of relevant neuroactive compounds or ions in the cleft. Prior studies of hair cells *in situ* are consistent with a systematic elevation of K^+ in the cleft following hair cell depolarization (Contini, 2011; Lim *et al.* 2011; Contini *et al.* 2012). Such results would obtain regardless of the source of K^+, and under the conditions of our experiment, with the hair cell at –70 mV, we would expect a continuous efflux of K^+ from the hair cell, and depolarization of the afferent might contribute additional K^+ or simply change the rate of its removal. In either case, we would expect $[K^+]_{\text{cleft}}$ to be elevated, which could change the equilibrium potentials and permeation through multiple presynaptic and postsynaptic channels facing the cleft.

K^+ efflux from the hair cell is necessary to generate the inward afferent current

We sought to block the hair cell potassium current to determine whether it was necessary to elicit the slow net inward current in the afferent (Fig. 3*A*). As in previous studies, simple substitution of Cs^+ for K^+ in the pipette was insufficient to block the potassium currents (Rennie & Correia, 2000). Na^+ was chosen as the intracellular cation and 20 mM 4-AP and 30 mM tetraethylammonium (TEA) were included in the recording pipette to block

residual K^+ currents. Internal solution of this composition efficiently blocked all but 1–2% of outward potassium currents in the hair cell. The residual current had slow activation kinetics ($\tau > 4.5$ ms) (Fig. 3*A*, upper traces) and the *I–V* curve was consistent with it being residual IK_{LV} (Fig. 3*A*, inset). Under these conditions, a 20 pA modulation in the holding current in the calyx remained (23.7 ± 18.6 pA, $n = 6$) (Fig. 3*A*, lower traces), a reduction of up to 98% from the value typically observed when recording pipettes were filled with K^+. The absence of an inward current in the afferent under these conditions suggests that elevation in $[K^+]_{cleft}$ resulting from hair cell K^+ efflux is necessary to generate the current. Also visible in the afferent recordings are EPSCs, indicative of ongoing vesicle fusion and transmitter release. However, since in this case their rate was constant and not dependent on hair cell depolarization, we have no evidence that the observed release of the large EPSCs was associated with the hair cell from which we were recording. Reconstruction of the pair revealed a dimorphic unit comprising a single complex calyx with five type I hair cells, as well as a single bouton ending, convergent onto the parent afferent. In principle, the observed quantal release might have been associated with any of these hair cells and their synapses. To verify that the afferent had not been compromised, a series of hyperpolarizing and depolarizing steps from a holding potential of –100 mV were applied to the afferent (Fig. 3*B*), again eliciting currents typical of vestibular afferents, including TTX-blockable APs when depolarized above –60 mV. The frequency of APs increased and their amplitude decreased with depolarization, reinforcing the notion that they are due to one of the multiple afferent Na^+ conductances (Liu *et al.* 2016) elicited by more proximal AP generation at the spike initiation zone. Unlike our prior results (Fig. 2*D*), with block of the hair cell potassium conductances, neither outward nor inward currents in the afferent modulated the resting current in the hair cell (Fig. 3*B*).

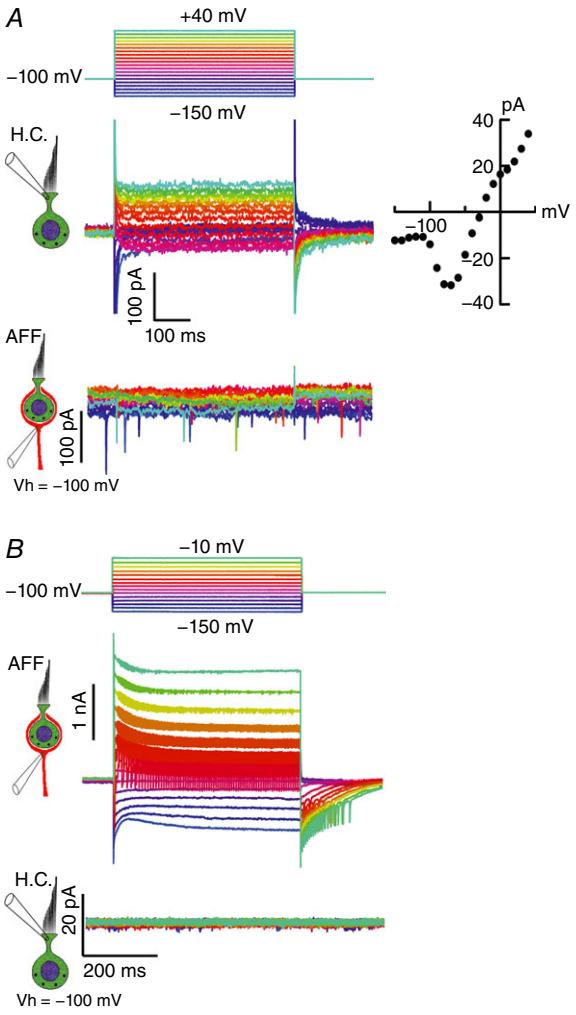

Figure 3. Blocking potassium flux from the hair cell blocks the slow inward current in the afferent neuron
A, potassium flux was blocked by substituting (mM) 80 Na^+, 20 4-AP and 30 TEA for K^+ in the recording pipette. Remaining 1% of typical hair cell current observed for K^+-filled electrodes is shown as the inset *I–V*. The slow inward current in the afferent was suppressed, although large EPSCs persist. *B*, afferent currents can be elicited by depolarizing and hyperpolarizing current steps. I_h is visible for the largest hyperpolarizations. No currents are induced in the hair cell as a result of depolarizing or hyperpolarizing the afferent neuron.

Elevation of potassium in the synaptic cleft results from depolarization of either the presynaptic hair cell or the postsynaptic afferent

For a hair cell enveloped by its afferent, the majority of its conductances are exposed solely to the ion concentrations in the cleft. As a consequence, the hair cell currents in the steady state and upon repolarization could be used to estimate the $[K^+]_{cleft}$. The first series of experiments (Fig. 4) tested the ability of hair cell depolarization to elevate $[K^+]_{cleft}$. With the afferent at –100 mV, and the hair cell at –70 mV, the hair cell was depolarized for 10 ms to 20 mV, and then repolarized to establish the control condition (Fig. 4*A*, left). The measured currents upon repolarization and 25 ms later were used to estimate the instantaneous (filled circles) and steady-state (open circles) *I–V* curves (Fig. 4*B*). After the repolarization, the hair cell was depolarized to 20 mV for 250 ms to produce a large outward current into the cleft, and the repolarization series repeated (Fig. 4*A*, right). The linear instantaneous *I–V* curve (Fig. 4*B*, filled squares) demonstrated an increased slope from 19.7 to 25.7 nS, and a systematic shift to the right. Based on the Nernst potentials, such a shift in the reversal potential is consistent with an elevation of $[K^+]_{cleft}$ from 10.9 to 18.9 mM. Measurement at 25 ms after repolarization (open squares) yielded an *I–V* curve that largely overlapped the initial control *I–V* curve, and it was only after 50 ms of repolarization (open squares) that the *I–V* curve had the rectifying form seen in the control

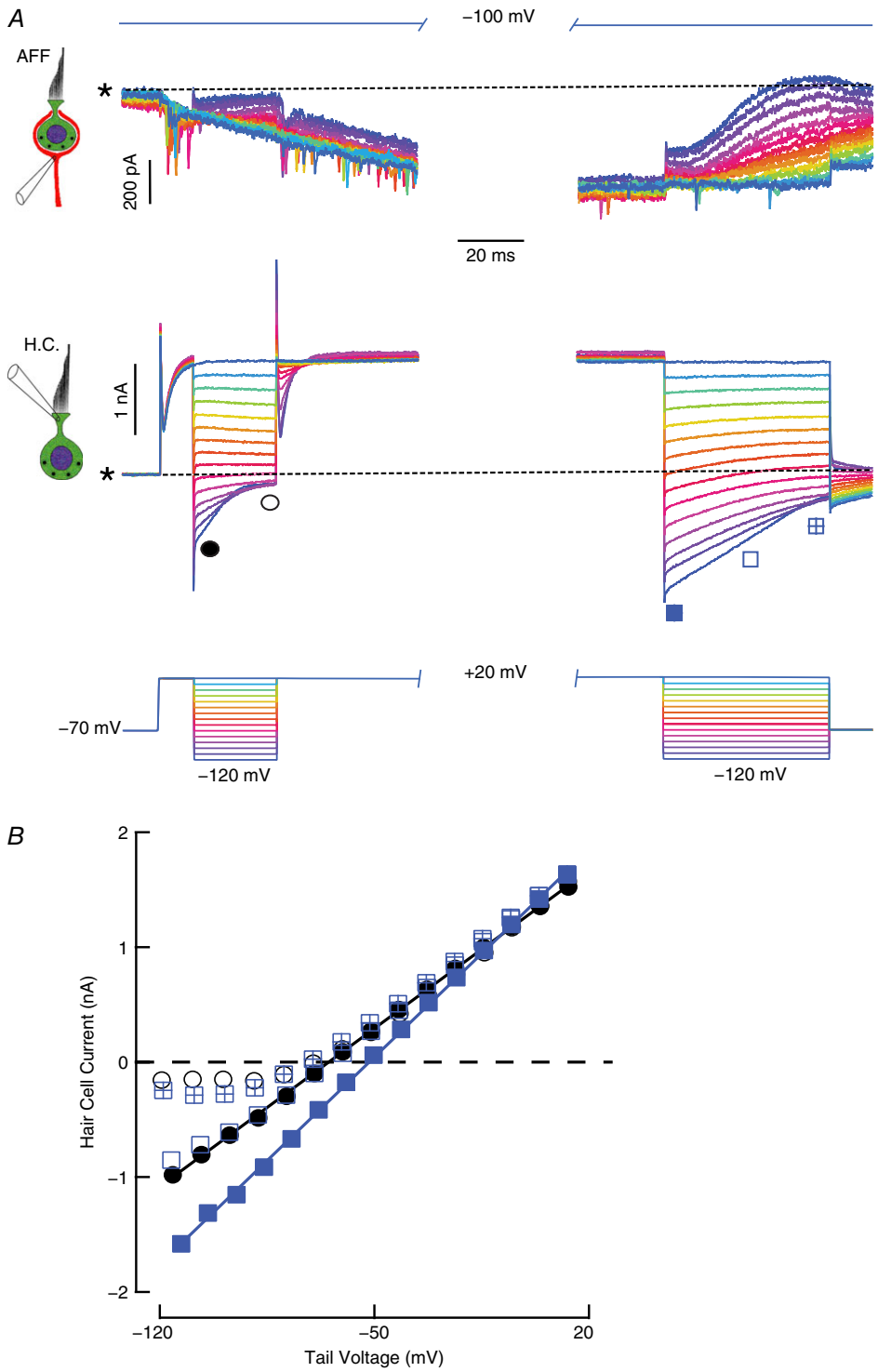

Figure 4. Potassium accumulation in the cleft resulting from depolarizing the hair cell
A, repolarization protocol before and after prolonged hair cell depolarization, with the afferent held at –100 mV. Tail currents upon repolarization from a 10 ms depolarization to 20 mV (left traces) close more rapidly than those after a 250 ms depolarization (right traces). *B*, after 10 ms depolarization, the instantaneous (filled circles) and steady-state (open circles) *I–V* curves for repolarization at the points indicated on the left traces of *A*, and after 250 ms depolarization, the instantaneous *I–V* curve (filled squares), that following 25 ms repolarization (open squares), and after 50 ms repolarization (crossed blue squares) for points indicated on the right traces of *A*. Asterisk and dashed line indicate the zero current level in the hair cell and a constant inward current of 2.695 nA in the afferent.

steady-state *I–V* curve. Note that during the prolonged hair cell depolarization, EPSCs were visible, a slow net inward current developed in the afferent, and with the subsequent hair cell hyperpolarizations, a corresponding series of net outward currents were evoked in the afferent, consistent with our prior experiments (Fig. 2*C*).

A second series of experiments (Fig. 5) was designed to examine whether depolarization of the afferent would produce a similar elevation of $[K^+]_{cleft}$. The potassium concentration was estimated as before, using the effect on the hair cell tail currents. The afferent was held at –100 mV, and the hair cell at –70 mV. The initial test (Fig. 5*A*, left) repeated the hair cell repolarization protocol from Fig. 4*A*, to generate the instantaneous (filled circles) and steady-state (open circles) *I–V* curves (Fig. 5*B*). At the end of the repolarization step, the hair cell was returned to –70 mV and the afferent depolarized to 0 mV for 245 ms to generate an outward current. Before the afferent was repolarized, the hair cell protocol was repeated (Fig. 5*A*, right), and the instantaneous (filled squares) and steady-state (open squares) *I–V* curves obtained. As with hair cell depolarization, the depolarization of the afferent resulted in an increase in hair cell conductance from 16.2 to 21.2 nS and a rightward shift in the instantaneous repolarization *I–V* curve that is consistent with an increase in $[K^+]_{cleft}$ from 10.9 to 26.6 mM.

In addition, for the protocols in both Figs 4 and 5, the rate of relaxation of the hair cell current upon repolarization was dramatically slowed in the presence of elevated potassium. In each control case, for the the largest hyperpolarization to –120 mV, the current deactivated with $\tau = 8.56$ ms. When the $[K^+]_{cleft}$ was elevated by prolonged depolarization of the hair cell, deactivation slowed to $\tau =$ 581.2 ms. In the case of $[K^+]_{cleft}$ elevation by the afferent, there was little relaxation in the current during the repolarization; the initial inward current of 1.07 nA decreased linearly at 4.2 pA per millisecond. As a consequence, the instantaneous and steady-state *I–V* curves largely overlapped (Fig. 5*B*). Our conclusion from these experiments is that depolarization of either hair cell or afferent will elevate the $[K^+]_{cleft}$. Further, the slowing of tail current time constant extends previous observations (Contini *et al.* 2012) and suggests that in addition to any inherent voltage sensitivity in the gating of the hair cell potassium conductances, one or more of them are sensitive to $[K^+]_o$ as well.

Quantifying the change in hair cell conductance and potassium equilibrium potential

To examine dynamic changes in $[K^+]_{cleft}$ associated with depolarization, both hair cell and afferent were held at –100 mV. Prior experiments on solitary hair cells bathed in low $[K^+]_o$ suggested that the major hair cell K^+ conductances are deactivated at this potential (Meredith & Rennie, 2016). In the afferent the inward current is dominated by an HCN conductance underlying the previously demonstrated I_h (Fig. 2*D*) (Chabbert *et al.* 2001; Meredith *et al.* 2012). In vestibular ganglion cells, the most highly expressed HCN subunit is HCN2, followed by HCN1 and HCN4, as assessed by RT-PCR and immunohistochemistry (Horwitz *et al.* 2014). HCN2 is a mixed conductance, with a sodium permeability/potassium permeability of between 0.41 and 0.47 in a heterologous expression system, when $[K^+]_o$ varied from 5.4 to 30 mM (Moroni *et al.* 2000). At –100 mV the driving force on Na^+ and K^+ would be 183 and 11 mV, respectively. Since the K^+ efflux from the hair cells is minimized at this potential, much of the standing inward current into the afferent will draw the bulk perilymph into the synaptic cleft and be carried by Na^+.

When depolarized from –100 mV the hair cell current activated sigmoidally, reaching a peak at 23 ms (Fig. 6*A*, expanded in Fig. 6*B*), before relaxing to the steady state. In the afferent, the depolarization of the hair cell was associated with a slowly developing inward current, upon which were occasional rapid EPSCs (Fig. 6*A*, expanded in Fig. 6*B*, arrows, bottom traces). The kinetic difference between the rapidly activating outward current in the hair cell and the slower activation of inward afferent current is consistent with the afferent current being proportional to a concentration change in the cleft, rather than the hair cell current itself. Repolarization of the hair cell elicited a large inward tail current that decayed slowly with a complex time course, dominated by a slow exponential decay: $\tau = 86.9 \pm 106.03$ ms, $n = 30$. The corresponding afferent relaxation at the end of the pulse was multiphasic as well, with an initial jump due to the uncompensated access resistance, followed by a decay with a dominant time constant: $\tau = 64.9 \pm 63.7$ ms. Hair cells also have a rapidly activating I_{Ca} ($\tau \leq 500$ μs at –20 mV) (Bao *et al.* 2003), and in preparations with the best electrode compensation, its value could be estimated at the end of the capacity transient associated with depolarizing steps (Fig. 6*B*, arrow, top traces), prior to the delayed onset of the combined I_K. For potentials hyperpolarized to –80 mV, the hair cell had a conductance of 2.26 nS (3.16 ± 2.30 nS, $n = 26$), indicated by the linear best fit (Fig. 6*C*), which was much less than the resting conductance of 39.7 nS for this cell at –70 mV. An inward U-shaped deviation from straight-line fit was apparent for potentials depolarized to –60 mV, which had a voltage range that was slightly more hyperpolarized than previously reported (Bao *et al.* 2003).

To characterize the changes in hair cell conductance and the reversal potential, the *I–V* curves for the hair cell at the end of a 500 ms pulse were measured in the steady state and after the transition to the holding potential. In the steady state the *I–V* curve was outwardly rectifying, with high impedance at hyperpolarized potentials (Fig. 6*D*, black circles). Upon repolarization to the holding potential, the

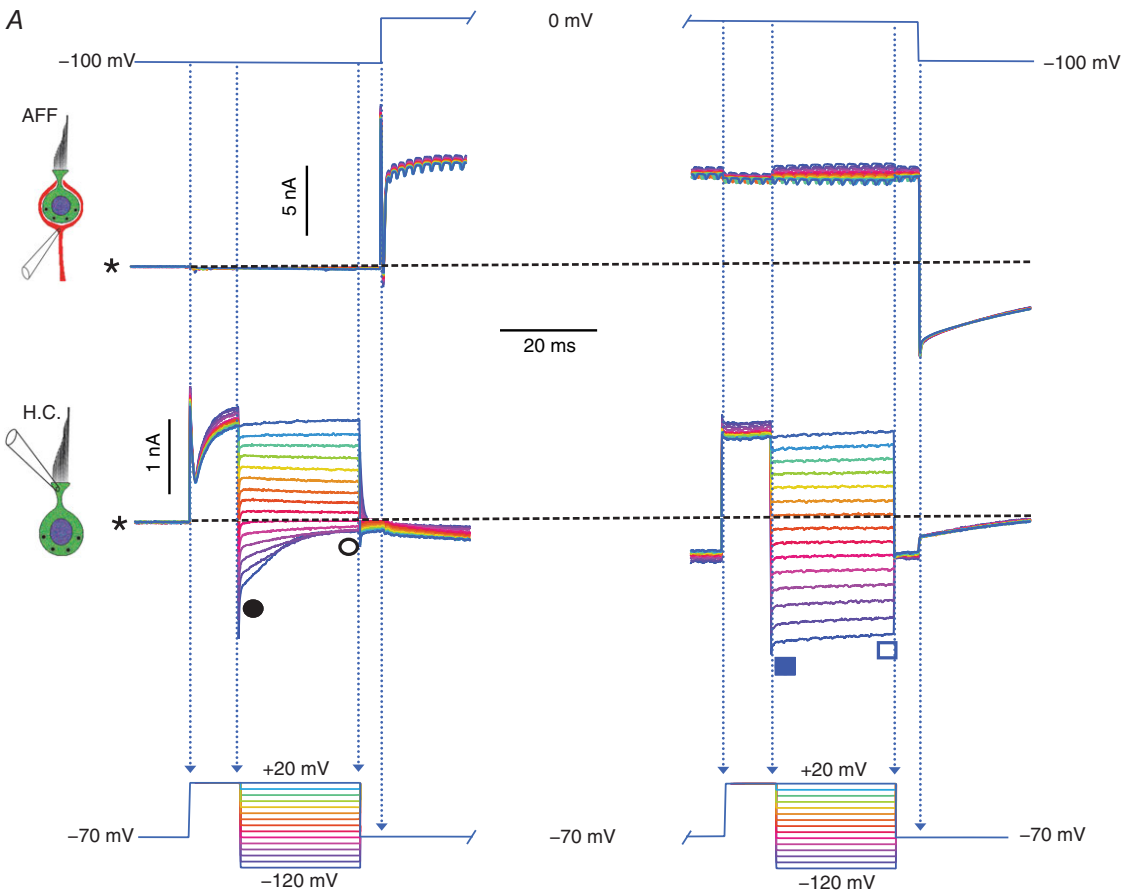

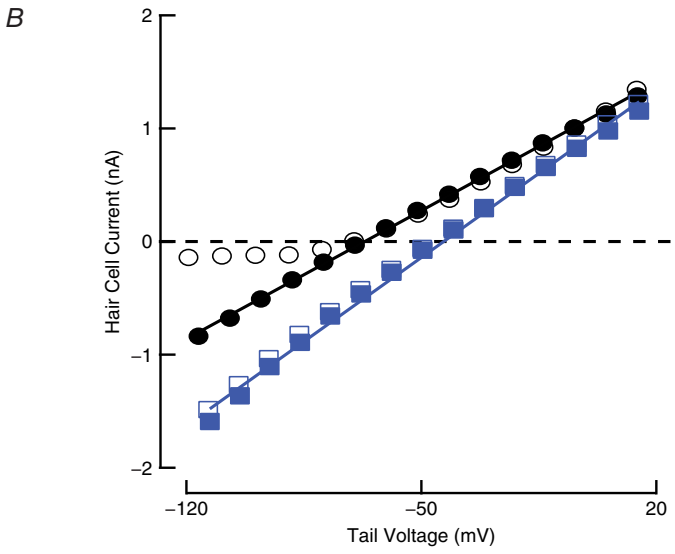

Figure 5. Potassium accumulation in the cleft resulting from depolarizing the afferent fibre
A, repolarization protocol before and after prolonged afferent depolarization. With the afferent held at –100mV, the hair cell tail currents upon repolarization from a 10 ms depolarization to 20 mV (left traces) close rapidly. After 245 ms afferent depolarization to 0 mV, the tails following a 10 ms depolarization to 20 mV remain largely open even after 25 ms (right traces). *B*, after 10 ms depolarization, the instantaneous (filled circles) and steady-state (open circles) *I–V* curves for repolarization at the points indicated on the left traces of *A*, and after 245 ms afferent depolarization, instantaneous *I–V* curve (filled squares), and that following 25 ms repolarization (open squares) for points indicated on the right traces of *A*. Asterisk and dashed line indicate the zero current level in the hair cell, and a constant inward current of 2.703 nA in the afferent.

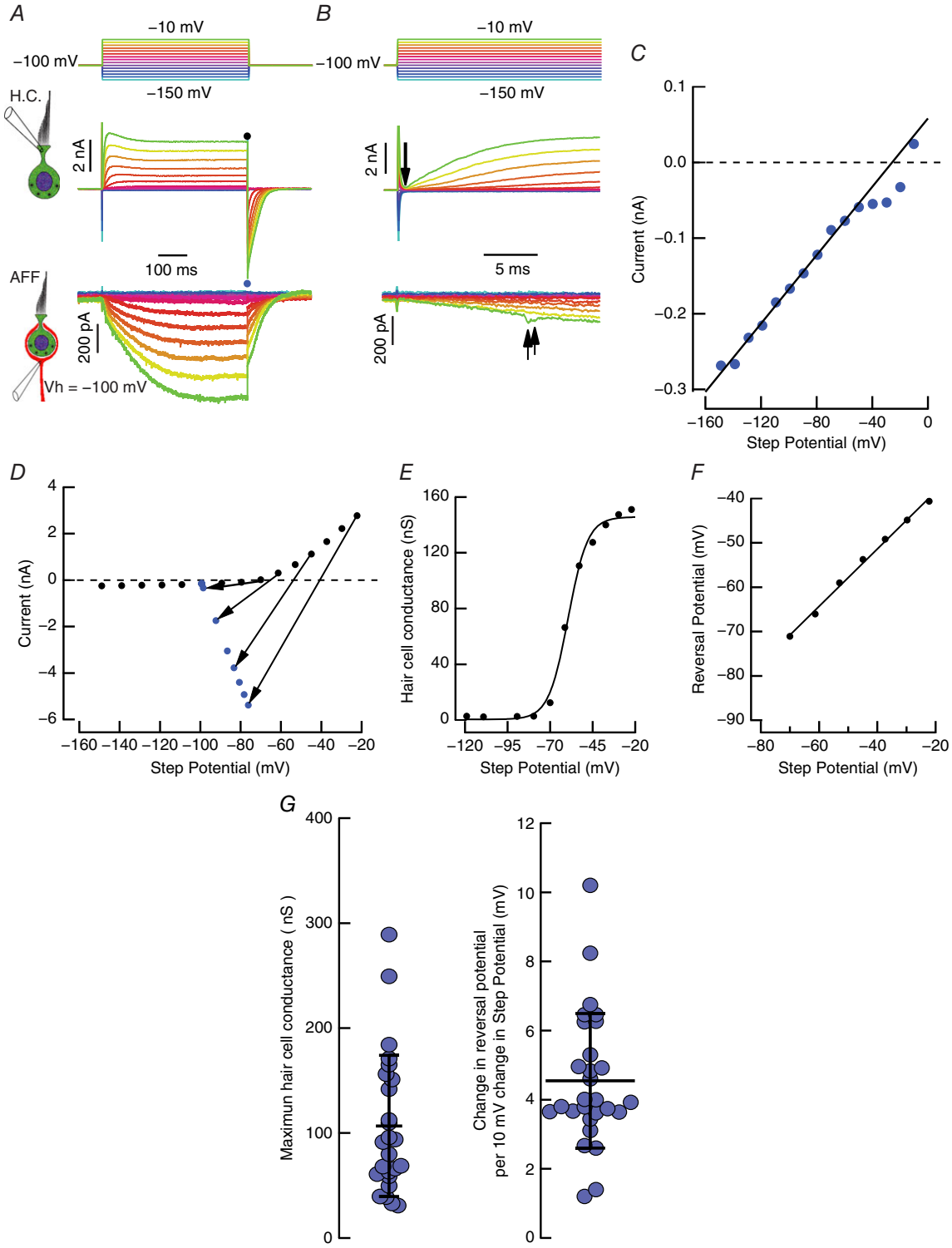

Figure 6. Analysis of chord conductances and reversal potential of hair cell current based on the steady-state and tail currents

A, voltage-clamp series applied to hair cell. Both hair cell and afferent were held at –100 mV. *B*, expanded view of the initial 25 ms of the responses in panel *A*. Arrow indicates a sampling point at 3× the electrode time constant, $\tau \approx 35\ \mu s$. *C*, instantaneous hair cell *I–V* relationship at time point indicated by the downward arrow in panel *B*. Current deviations from the regression line for voltages depolarized to –60 mV were used to estimate I_{Ca}. *D*, the steady-state current (black circles), and the peak tail current after the capacity transient (blue circles) are plotted

for each voltage. The slope of lines connecting corresponding steady-state and tail currents are the conductance at the moment of transition. The point at which each line intersects the zero-current axis is the reversal potential. *E*, chord conductances plotted against the corrected step potential. Conductances fit with a sigmoid function. *F*, reversal potentials plotted against the step potential. For depolarizations, the reversal potential *vs*. step potential is well fit by a line corresponding to a shift of 3.15 mV for each 10 mV of depolarization. *G*, aggregate conductance and reversal potential scatter plots at –100 mV. The maximal conductance averaged 106.74 ± 67.23 nS ($n = 25$), and the rate of shift in the reversal potential for each 10 mV of depolarization was 4.54 ± 1.95 mV ($n = 28$).

peak tail current was a linear function (Fig. 6*D*, blue circles). Calculation of the potassium conductance and driving force on potassium ions at the end of the pulse were derived from the lines connecting the steady-state and tail currents at each voltage (Adelman *et al.* 1973). In the usual way, we assumed that at the moment of repolarization the conductance and the driving force for the current were unchanged. With this assumption, the arrows connecting the steady-state current to the peak of the tail current could be used to estimate the conductance and equilibrium potential. The slope of the line corresponded to the steady-state conductance, and the point at which the line intersected the zero-current axis was an estimate of the reversal potential. Two features should be noted. Firstly, the slope of the line, and therefore the hair cell conductance, increased with increased depolarization. Secondly, with larger depolarization, the point at which the line intersected the zero-current axis was shifted progressively to the right, consistent with a change in driving force.

When held at –100 mV, the hair cell conductance reached a maximum of 151 nS, and was fit by a sigmoid function (Fig. 6*E*). The corresponding changes in the reversal potential with voltage (Fig. 6*F*) increased linearly by 3.2 mV per 10 mV of hair cell depolarization, reaching a maximum of –39.87 mV for a depolarization to –22.2 mV. For this example, the change in reversal potential by 26 mV would be consistent with an increase in $[K]_{cleft}$ from 8.3 to 22.8 mM. The aggregate data for maximum conductance and the rate of change in the reversal potential for such pairs held at –100 mV is given in Fig. 6*G*.

The slowly developing current in the afferent is sensitive to HCN channel blockers

Superimposed on hair cell-induced inward current in the afferent were CNQX-sensitive quantal events typical of both the auditory and vestibular systems (Rutherford *et al.* 2012; Sadeghi *et al.* 2014; Fuchs & Glowatzki, 2015). To identify the afferent conductances that were modulated by hair cell depolarization, the paired experiment was repeated (Fig. 7*A*), eliciting both the slow inward current and faster quanta. To determine whether the inward current had a component attributable to an accumulation of glutamate, and mediated through previously characterized AMPA receptors, the experiment was repeated in the presence of 20 μM CNQX, an AMPA receptor (AMPAR) inhibitor (Fig. 7*B*). Depolarization of the hair cell resulted in a slow inward current in the afferent, but the large high-frequency EPSCs were blocked (Fig. 7*B*, lower traces). The afferent responses for the two largest traces in Fig. 7*A* and *B* are shown overlaid and subtracted in Fig. 7*D*. Consistent with prior results (Highstein *et al.* 2014), fast events but not the slow inward current were AMPAR mediated. To determine the permeation pathway for the inward current in the afferent, the experiment was repeated with both CNQX and 200 μM ZD7288, an irreversible blocker of the HCN channels (Fig. 7*C*) (Gasparini & DiFrancesco, 1997; Shin *et al.* 2001). With the addition of ZD7288, half of the standing inward current, and 85% of the current elicited with maximal hair cell depolarization were blocked. The afferent currents shown for maximal hair cell depolarizations in Fig. 7*B* and *C* are expanded in Fig. 7*E*. The voltage-dependent block of HCN (Shin *et al.* 2001) is typical of the values reported for similar concentrations of ZD7288 in prior vestibular experiments (Meredith *et al.* 2012; Kim & Holt, 2013). The use of CNQX and ZD7288 had minimal direct effect on the steady-state presynaptic currents, as can be appreciated by the overlap in the hair cell steady-state *I–V* curves (Fig. 7*F*). It should also be noted that in the presence of CNQX and ZD7288 the dominant time constant of relaxation in the tail current, $\tau = 20.9$ ms, was nearly twice that of the value in control or CNQX alone (average $\tau = 12.1$ ms), suggesting that $[K^+]_{cleft}$ remained elevated when afferent HCN channels were blocked. The steady-state *I–V* curves for the postsynaptic afferent, at the end of the depolarizing step in the hair cell, showed the ZD7288 block of both the standing inward current and the component elicited by depolarization of the hair cell (Fig. 7*G*).

The fact that CNQX failed to block afferent slow inward currents does not preclude the possibility that other substances released from the synaptic vesicles may be partially responsible for the effect. Vesicle fusion would be associated with a decrease in $[H^+]_{cleft}$, and it has been suggested that this might generate an inward cation current acting through an ASIC (Highstein *et al.* 2014). To address this issue we sought to limit dynamic changes in $[H^+]$ by increasing the buffer from 10 mM to 40 mM Hepes at pH 7.6 (Fig. 8). This resulted in increased currents in both the hair cell and the afferent (Fig. 8*B*). In the hair cell, increased buffering resulted in a larger inward calcium current, I_{Ca} (Fig. 8*F*), which was consistent with a reduction in the H^+ block of the Ca^{2+} channel that has

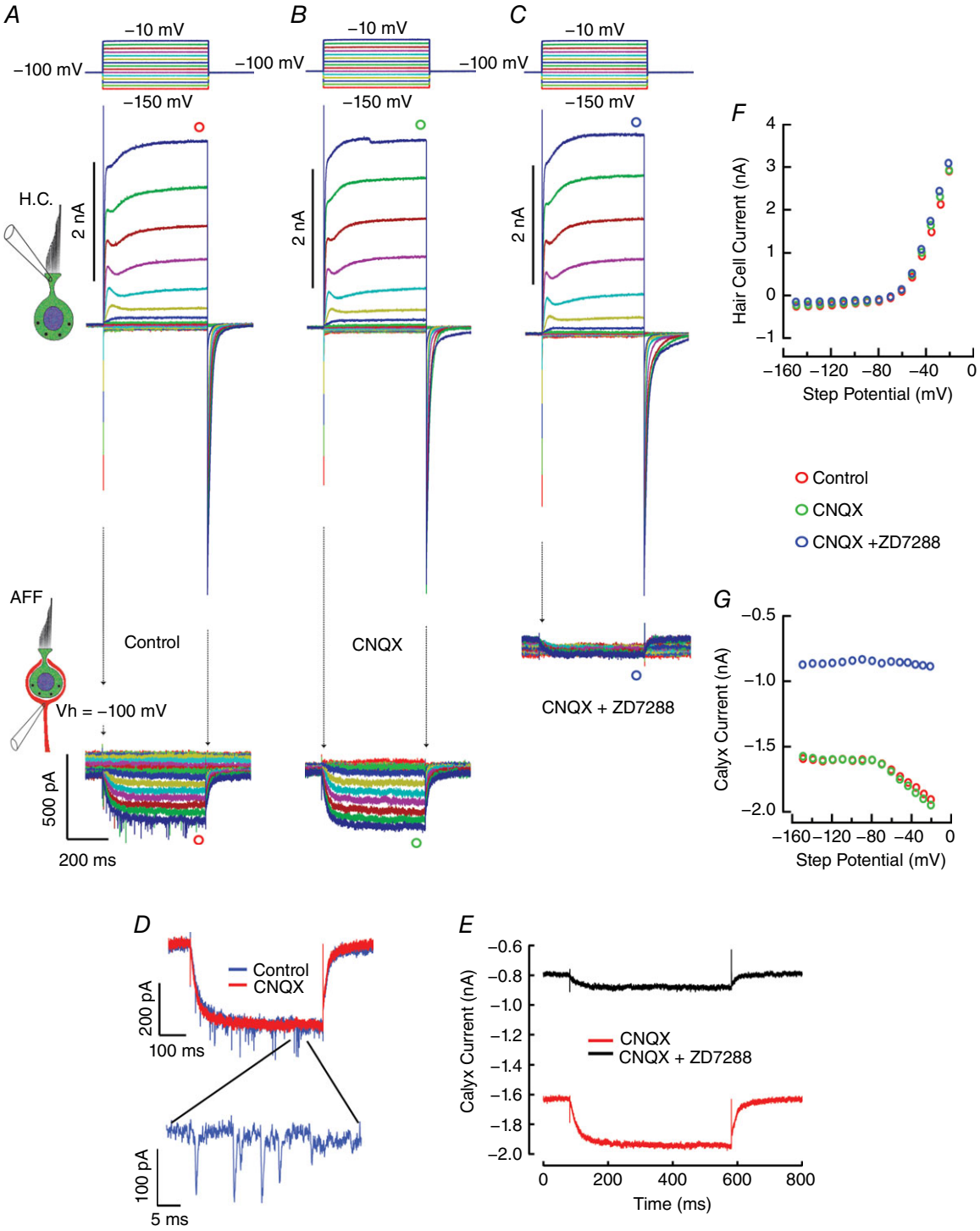

Figure 7. Response of the hair cell and afferent neuron pair to application of AMPAR and HCN blockers
A, with hair cell and afferent clamped at –100 mV, depolarization elicits outward current from the hair cell, with the slow inward current and EPSCs elicited in the afferent neuron. *B*, the experiment in the presence of 20 μM CNQX eliminates the large rapid EPSCs, but the slow inward current remains. Afferent response for the two largest traces from *A* and *B* are shown overlaid and expanded in panel *D*. *C*, addition of 200 μM ZD7288 to CNQX results in a decrease in the standing inward current in the afferent, as well as a reduction of 85% in the response elicited by hair cell depolarization. Afferent currents for maximal hair cell depolarizations in *B* and *C* are shown in expanded view in panel *E*. *F*, steady-state *I–V* curve for presynaptic hair cell at the end of the depolarizing step under the three conditions. *G*, steady-state *I–V* curve for postsynaptic neuron at the end of the depolarizing step in the hair cell under control and in the presence of CNQX and ZD7288.

been reported in the visual (DeVries, 2001) and auditory (Cho & von Gersdorff, 2014) systems. The increase in the outward current under these circumstances by 50.3% (24.4 ± 18.3%, $n = 4$) would be consistent with an increase in the size of a previously reported hair cell calcium-activated potassium current (IK_{Ca}) (Rennie & Correia, 1994; Schweizer *et al.* 2009). In addition to the relief of the H^+ block of the I_{Ca}, increased buffering would relieve the direct H^+ block of the BK channels (Church *et al.* 1998). The greater than proportional increase in the

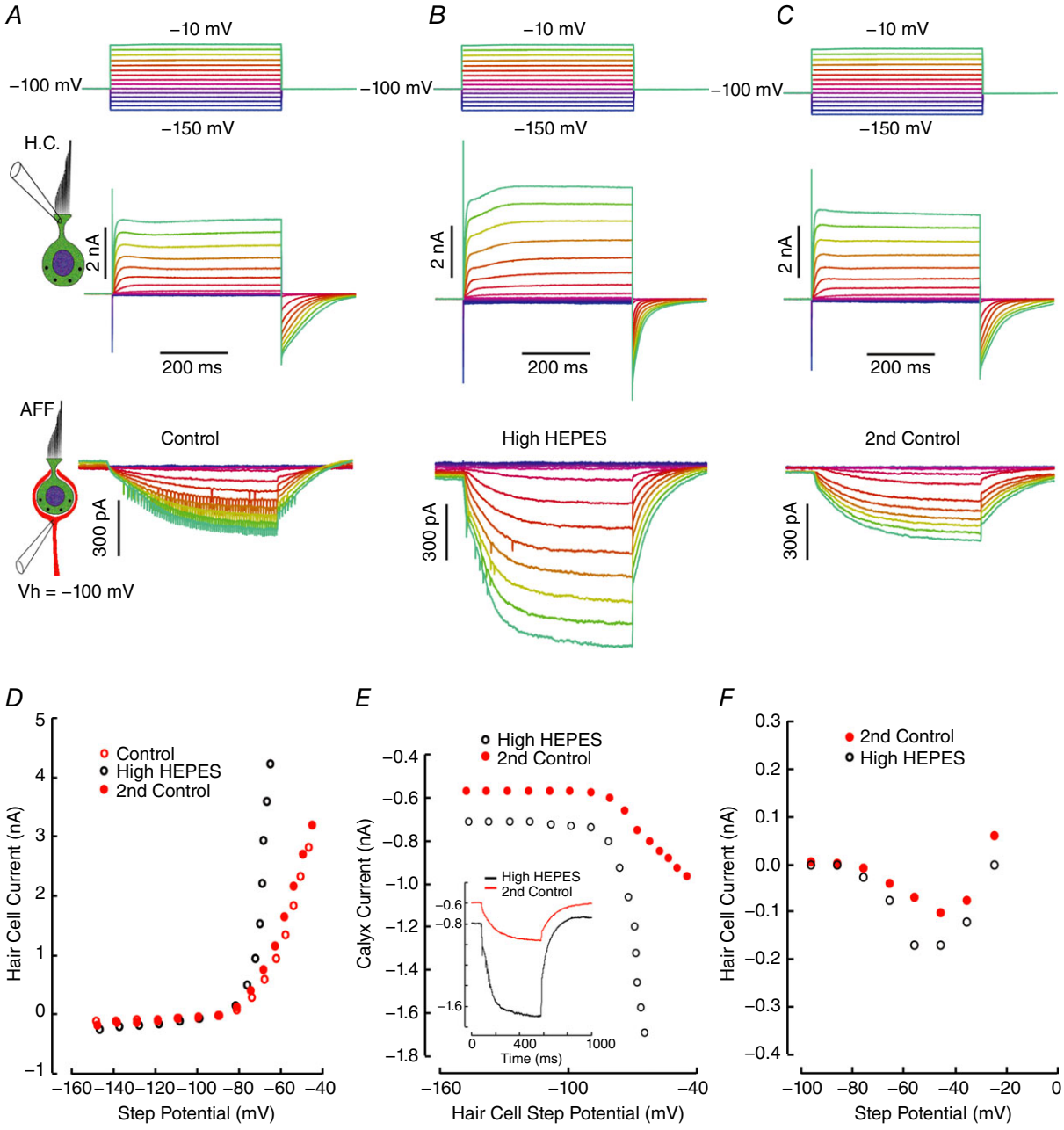

Figure 8. Effect of increased pH buffering on hair cell and afferent responses
A, hair cell and afferent responses to voltage steps in 10 mM Hepes (control). Decay of tail current, $\tau = 62.6$ ms. *B*, series repeated in 40 mM Hepes. Hair cell outward current and the induced inward current increase. Decay of the tail current, $\tau = 34.3$ ms. *C*, subsequent return control in 10 mM Hepes. Decay time constant, $\tau = 61.6$ ms. *D*, steady-state hair cell current in 10 mM Hepes (control), and in 40 mM Hepes (High Hepes). *E*, effect of $[Hepes]_o$ on afferent *I–V* curve induced by depolarization of the hair cell in 10 mM (filled circles) and 40 mM Hepes (open circles). Inset, maximal afferent response to depolarization of the hair cell in normal (10 mM) and high Hepes (40 mM). *F*, inward calcium current *I–V* curve (measured as in Fig. 6*C*) under normal (filled circles) and high Hepes (open circles).

inward current by 115.9% (33.9 ± 54.8%, $n = 4$) in the afferent suggests an additional postsynaptic effect on the HCN channels via their modulation by extracellular and intracellular $[H^+]$ (Munsch & Pape, 1999; Zong *et al.* 2001; Cichy *et al.* 2015). Of note is a more rapid decay of the hair cell tail current with increased buffering, changing from a control value of $\tau = 62.6$ ms in 10 mM Hepes to $\tau = 34.3$ ms in 40 mM Hepes, suggesting that larger inward tail currents in both hair cell and afferent decreased the $[K^+]_{cleft}$ more rapidly. In the context of normal transmission, with relatively low H^+ buffering capacity in the cleft (Highstein *et al.* 2014), elevated rates of vesicle release would decrease the cleft pH. This would create a negative feedback mechanism via $[H^+]$ to diminish both presynaptic and postsynaptic currents, thereby decreasing the elevation of $[K^+]_{cleft}$, and limiting depolarization.

Implication of K^+ modulation of afferent potential on transmission across the synapse

Additional studies addressed the second component of the afferent response elicited by depolarization of the hair cell (Fig. 2*A*, lower traces), the generation of APs associated with larger afferent depolarization. It is of singular importance in the context of the present study that quantal synaptic transmission between hair cell and afferent includes a population of large, rapid EPSCs (Fig. 9*A*). Afferent recordings revealed EPSCs of striking irregularity in the interval between events, and a wide range of amplitudes (Fig. 9*B*). For the afferent illustrated, amplitudes ranged from 50 to 400 pA, with a mean of 153 pA at –70 mV (Fig. 9*C*). Across the population the mean amplitude of the EPSCs was 99 ± 40.2 pA ($n = 15$), and the range of the smallest and largest 4% of events extended from a discernible minimum of 32 ± 9.1 pA to a maximum of 233 ± 91 pA (Fig. 9*D*). As outlined in Methods, the variation in timing between events was quantified using the coefficient of variation (CV), the ratio of the standard deviation of the inter-event interval to the mean interval between events (Fig. 9*E*). For each afferent the CV is a power function of the mean rate, and decreases as the interval between events shortens. The relationship for one such analysis is shown as the continuous line that is the best fit for an afferent whose CV was 1.28 at 47.4 ms mean interval. As the rate of events increased, the CV was reduced to 0.67 at a mean interval of 2.8 ms. The intervals were more irregular, with CVs ranging between 0.53 and 1.88 ($n = 16$) than the afferent discharge in the intact preparation (Brichta & Goldberg, 2000*a*). The large number of ribbons presynaptic to the afferent neuron (Goldberg *et al.* 1990) precludes addressing whether the variation in EPSC amplitude and timing is due to their being sourced by different hair cells or to different synaptic sites of a given hair cell (Highstein *et al.* 2015). Additionally, such variation in EPSC amplitude might arise from differences in vesicle size (Karunanithi *et al.* 2002), the kinetic profiles of fusion events (Photowala *et al.* 2006; Lisman *et al.* 2007), or the possibility of multi-vesicular fusion as has been suggested for auditory hair cells (Glowatzki & Fuchs, 2002).

The afferent response in current clamp (Fig. 9*F* and *G*) demonstrated the functional implication of modulating the resting potential. At a potential of –68 mV, none of the EPSPs reached a potential necessary for triggering a regenerative AP for transmission to the CNS. An additional 200 pA inward current was sufficient to depolarize the afferent to a potential of –63 mV, and generate APs from large single EPSPs, or coincident smaller ones (Fig. 9*H* and *I*). The APs arise from relatively few large EPSPs on a stable baseline, rather than from the summation of a large number of small quanta by a leaky integrate-and-fire neuron (Gabbiani & Koch, 2003). This implies that synaptic transmission is highly dependent on the potential, and to be effective the afferent must be kept within a few millivolts of threshold for generating APs (Goldberg & Holt, 2013). It is in just such a system, where single quantal events trigger APs, that high-frequency transmission is possible, and the rate of AP generation is determined by the timing and amplitude distribution of presynaptic release. Indeed, previous afferent data (Brichta & Goldberg, 2000*b*) suggest that calyx-bearing units are able to discharge at more than twice the rate of bouton-only afferents.

Comparison of type I and type II hair cell depolarization on the afferent response

Our primary focus in these experiments was on synaptic transmission between type I hair cells and their enveloping calyx. Occasionally, however, we achieved simultaneous recordings from a type II hair cell that synapsed onto the external face of the calyx. Comparison of the two configurations revealed differences in both hair cell and afferent responses (Fig. 10). Depolarization of a type I hair cell generated a rapid outward current through the large resting conductance, and in the afferent this elicited both EPSCS and a slow inward current (Fig. 10*A*). With sufficient inward current the largest EPSCs triggered TTX-blockable rapid inward currents in the afferent, indicative of AP generation (Fig. 10*A*, fourth, dark blue trace). Larger hair cell depolarization was associated with larger inward afferent currents that generated repetitive high-frequency discharge ranging from 75 to 193 Hz, with frequencies proportional to the amplitude of the inward current. By contrast, depolarization of a type II hair cell synapsing on the outer face of the calyx generated slowly activating outward current in the hair cell, and both EPSCs and a relatively modest inward current in the afferent (Fig. 10*B*). Increased depolarization of the hair cell increased the rate of EPSC generation, but even with

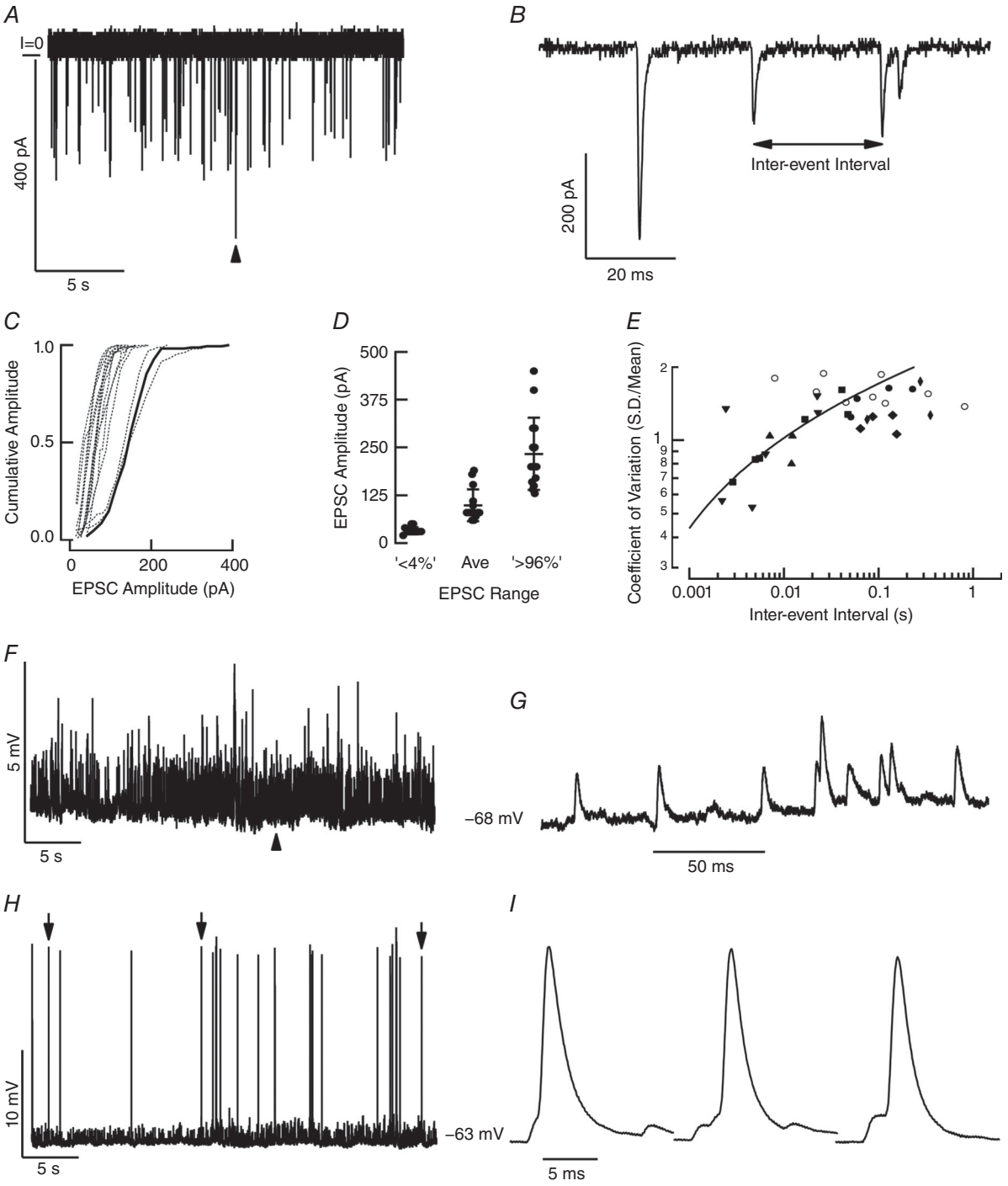

Figure 9. Behaviour of spontaneous quantal events
A, spontaneous EPSCs recorded in the afferent neuron. *B*, trace at arrowhead in panel *A* expanded to show variation in amplitude and timing of EPSCs. *C*, cumulative amplitude histograms of EPSC amplitude for 15 cells. Thick line indicates amplitude histogram of the afferent shown in *A* and *B*. *D*, average amplitude and that of the smallest and largest 4% of events for these cells. *E*, coefficient of variation (CV) for 16 cells. Continuous line is fit to a power function for a unit (filled squares) with a standardized CV* at 50 ms of 1.5. *F*, in current clamp, spontaneous EPSPs arise from a baseline of –68 mV. *G*, trace at arrowhead in panel *F* expanded to show unitary EPSPs. *H*, an inward current of 200 pA depolarized the afferent to –63 mV. Large action potentials arise from single, large EPSPs as well as from the summation of smaller, contemporaneous EPSPs. *I*, expanded traces, corresponding to downward arrows in panel *H* showing EPSPs giving rise to APs.

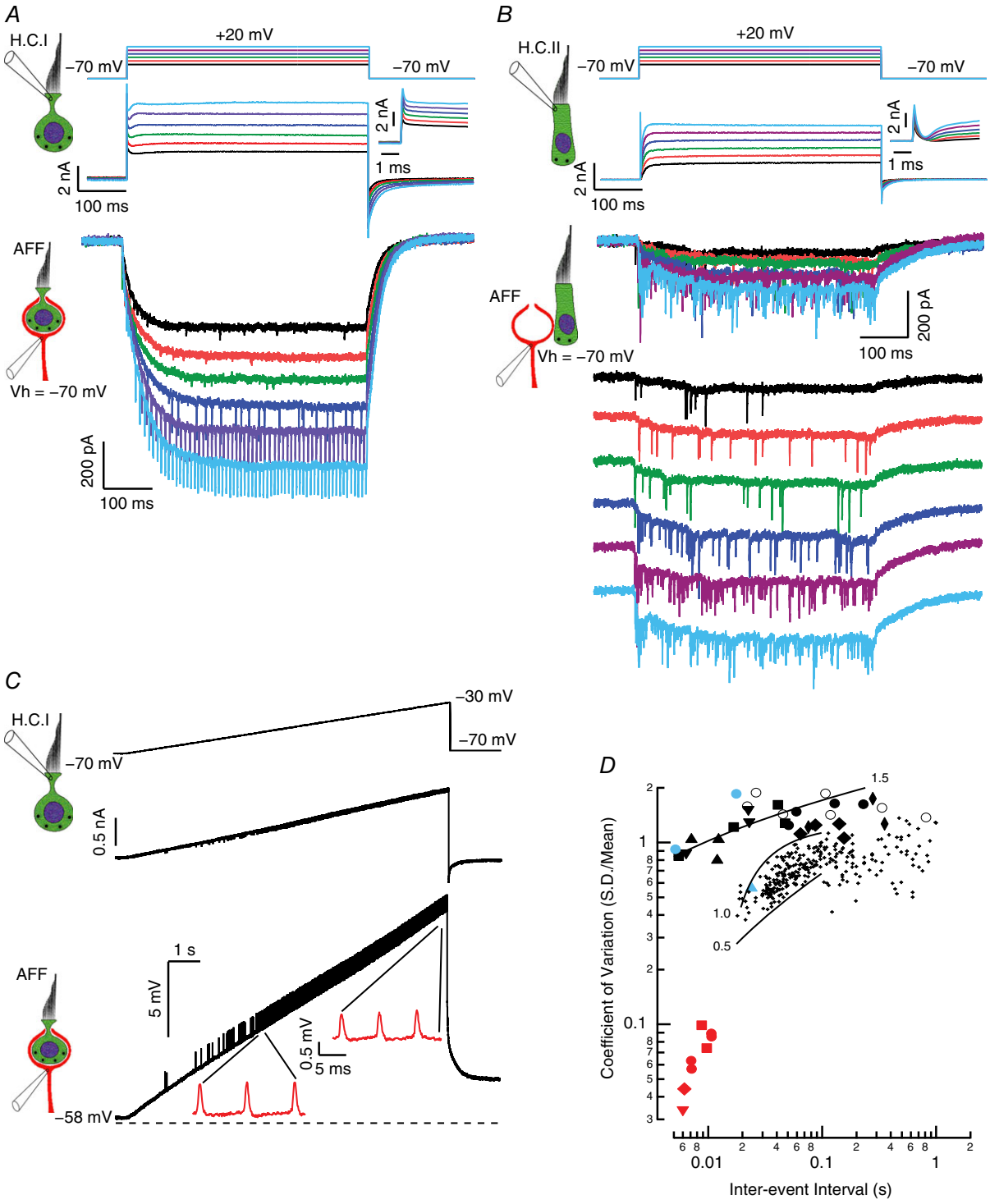

Figure 10. Comparison of depolarization of type I and type II hair cells on afferent response
A, rapid outward currents (expanded inset) result from depolarization of a type I hair cell. Slow inward currents and EPSCs are evoked in the afferent. In the fourth trace (dark blue) the largest EPSCs trigger TTX-blockable currents associated with generating APs. Larger inward currents give rise to high-frequency, evenly spaced discharge. *B*, outward currents (expanded inset) develop slowly upon depolarization of a type II hair cell. Large EPSCs are evoked in the afferent, with small, slow inward current with the largest hair cell depolarization. In the lower set of afferent traces, the afferent responses are displaced from each other by 200 pA, to reveal the increased EPSC frequency associated with hair cell depolarization. *C*, ramp depolarization of a type I hair cell in voltage clamp generated a ramp of outward current. This was associated with a depolarization of the afferent held in current

clamp. Continuous high-frequency discharge, 117 Hz (expanded) at –51.9 mV increased to 143 Hz (expanded inset) at –43.9 mV. *D*, coefficient of variation in the timing between events. The small points are data from Brichta & Goldberg (2000*a*) (adapted with permission from the American Physiological Society) and show regularity of calyceal and dimorphic afferents in the posterior semicircular canal of the turtle. Thin black lines are power functions delimiting units with CVs between 0.5 and 1.0. The large black symbols and thick black line are replotted from Fig. 9*E* and show the regularity of EPSCs and EPSPs in the current study for 16 cells. The large blue filled circles and triangle show evoked APs for two afferents. The red symbols show the regularity of high-frequency afferent discharge evoked by large inward currents.

maximal depolarization of the hair cell, none of the EPSCs triggered APs. In fact, the slow inward current of 75 pA produced by depolarizing the type II hair cell to –20 mV was far less than the 595 ± 451 pA ($n = 29$), produced by equivalent depolarization of type I hair cells.

High-frequency repetitive afferent discharge was universally observed in voltage clamp experiments when afferents were depolarized above –50 mV. The rate and the high degree of regularity suggested that afferents could be depolarized to voltages where intrinsic conductances would give rise to repetitive discharge. This afferent phenomenon could also be evoked by sufficient hair cell depolarization (Fig. 10*C*). Depolarizing voltage ramps to the hair cell elicited corresponding depolarizations of the afferents held in current clamp. When afferents were depolarized above –51.85 ± 3.80 mV ($n = 3$), regularly spaced, rapid TTX-blockable potentials were observed. The rate of discharge was proportional to the level of depolarization, and their regularity increased as the inter-event interval decreased. These results indicated that with sufficient hair cell depolarization, the K^+ efflux into the cleft was sufficient to drive the afferent to potentials with spontaneous discharge, which had interval statistics that were distinct from the activity evoked by large EPSPs. When the CVs for this mode of discharge were plotted with CVs derived from EPSCs, EPSPs and evoked APs of the present study, along with prior afferent data for dimorphic or calyceal afferents (Brichta & Goldberg, 2000), the difference in regularity was striking (Fig. 10*D*). In general, the inter-event interval was shorter than those reported previously. At a given inter-event interval, the repetitive discharge at voltages depolarized to –50 mV was more regular than prior afferent recordings, or our synaptic events and afferent discharge. By contrast, the regularity of our synaptic events and afferent discharge were within a factor of 2 of, and in many cases overlapped with, the regularity of the prior afferent study (Brichta & Goldberg, 2000).

Discussion

Our intent was to examine synaptic transmission and the modulatory effects of ion accumulation in the femtolitre intercellular space of the synapse, and to assess its effect on the function of both presynaptic and postsynaptic neurons. Our data support the notion that the $[K^+]_{cleft}$ varies dynamically, and departs significantly from its value in the bulk of the extracellular fluid. This modulation of $[K^+]_{cleft}$ shapes the characteristics of information transfer across the synapse, and may permit high-fidelity intercellular communication by maintaining both cells near their physiological thresholds for vesicle release and generation of an AP.

Substituting Na^+ for K^+ and adding potassium channel blockers, 4-AP and TEA, in the hair cell (Fig. 3) abolished the slow CNQX-insensitive afferent inward current, demonstrating that an efflux of K^+ into the cleft is necessary for the postsynaptic effect. Such K^+ efflux would elevate the $[K^+]_{cleft}$, and decrease the $[Na^+]_{cleft}$. At a minimum these changes would dynamically alter the equilibrium potentials for the hair cell and afferent channels facing the synapse. Our estimate of $[K^+]_{cleft}$ has relied throughout on an analysis of the slope and zero-current crossing of the instantaneous *I–V* curve upon repolarization of the presynaptic hair cell (Fig. 6). Hair cells of the central region are known to contain at least three outward potassium conductances (Meredith & Rennie, 2016). The impact of elevating $[K^+]_{cleft}$ on the specific equilibria potentials of the three will require detailed knowledge of their activation ranges and their relative permeability to K^+ and Na^+.

Implications of extended and close synaptic apposition on hair cell physiology

As articulated by Katz (1969), chemical synaptic transmission is a voltage- (Baylor & Fettiplace, 1976) and calcium-dependent (Llinas *et al.* 1976) cascade that leads to vesicle fusion and depolarization of the postsynaptic membrane. For hair cells with conventional bouton synapses, inward transduction currents through the apical pole flow outward across modest basolateral conductances, and the cell depolarizes to potentials sufficient to gate the influx of calcium necessary for vesicle fusion (Fig. 11*A*). The concern for hair cells enveloped by a postsynaptic afferent is that the basolateral conductances are very large at rest, and transduction currents alone would be insufficient to depolarize the cell to voltages necessary for synaptic transmission. As suggested previously (Chen, 1995; Goldberg, 1996*a*), a twist is that the depolarization could be achieved by the concerted actions of the transduction current and a decrease in the

driving force on basolateral potassium conductances due to the elevation of $[K^+]_{cleft}$ created by potassium efflux (Fig. 11*B*). In our experiments, hair cells in the resting state had reversal potentials for the outward current only a few millivolts hyperpolarized to their potential of –70 mV. As a hair cell was depolarized and currents flowed out into the cleft, the equilibrium potential shifted to more depolarized potentials, on average nearly a 0.5 mV shift for each millivolt of depolarization. In this way, one can imagine that a hair cell could be bootstrapped to potentials sufficient to gate a calcium influx necessary for vesicle fusion (Contini *et al.* 2012). This process would also be associated with a change in the hair cell basolateral conductance that will increase over time and, as was shown in Fig. 2*A* and *B*, produce a phasic voltage response even to an inward current that mimics a constant transduction current. This may well be a process occurring to some extent at all synapses, and for the vestibular system in particular, the magnitude of the effect of ion concentration will be correlated with the degree of anatomical overlap between presynaptic and postsynaptic cells.

Potassium modulation of postsynaptic conductances

There were obvious kinetic differences between the rapid outward current in the hair cell, and the slow inward

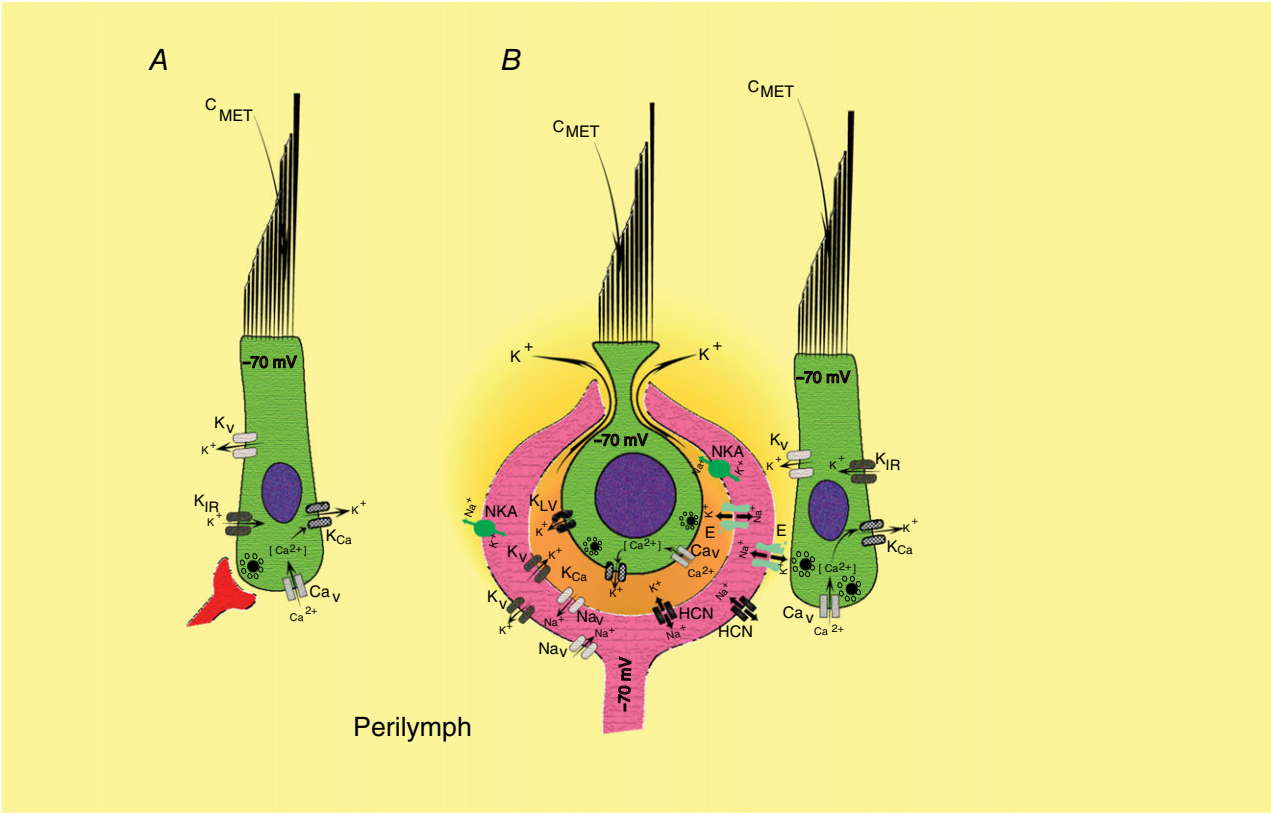

Figure 11. Schematic diagrams of synaptic transmission between type II and type I hair cells and their afferent fibres
A, type II hair cells with bouton endings are depolarized by cationic transduction currents through the mechanically sensitive bundle. Positive feedback to further depolarize the cell is afforded by I_{Ca} and the negative-slope region of I_{KIR} (Goodman & Art, 1996). Negative feedback is provided by I_K and IK_{Ca} that would repolarize the cell. *B*, type I hair cells within a calyx are depolarized by cationic transduction currents through the mechanically sensitive bundle. Positive feedback to depolarize the cell is provided by I_{Ca}, a glutamate transporter (not shown) (Dalet *et al.* 2012), and a shift in the K^+ equilibrium potential, due to K^+ accumulation in the cleft. The K^+ current efflux is primarily through low-voltage-activating K^+ channels (K_{LV}), calcium-activated K^+ channels (K_{Ca}) and high-voltage activating K^+ channels (not illustrated). Type II hair cells synapsing on the external face of the afferent function in a manner similar to that of type II hair cells onto boutons. For both internal and external face synapses, the afferent is depolarized by glutamate acting on AMPARs. Positive feedback to depolarize the afferent further results from the actions of non-inactivating Na^+ currents (I_{Na}), HCN channels (I_h) and possibly glutamate transporters. Negative feedback, tending to repolarize the cell, has contributions from a wide variety of K^+ channels (I_K) and activity of the Na^+/K^+-ATPase (NKA). Transporters and channels on the external face would experience relatively constant ion concentrations, while those on the inner face would change dynamically with activity.

afferent current. The latter was proportional to the integral of the presynaptic current, which is consistent with it being evoked by a systematic change in the ion concentration in the cleft, rather than ephaptic transmission between presynaptic and postsynaptic cells as has been described for adjacent nerve fibres (Katz & Schmitt, 1940). Synchronous potentials were observed with AP generation (Fig. 2*A* and *D*, and 5); however, we cannot distinguish whether these represent resistive coupling between the hair cell and afferent via the synaptic cleft, or an artifact of electrode coupling.

We could elicit inward currents or depolarizations in all hair cell–afferent pairs except on the occasion of recording from type II hair cells on the external face of the afferent. Under those conditions, we could modulate the quantal rate without eliciting large inward currents. The inward current was universally elicited by depolarization of type I hair cells, a result, however, at odds with prior single-electrode afferent recordings using mechanical stimulation of the ciliary bundle (Highstein *et al.* 2014). In an afferent with a complex calyx we expect the depolarizing effect of the enveloped hair cells to sum. As a result, the level of hair cell depolarization necessary for a given afferent depolarization should decrease by a factor proportional to the number of hair cells presynaptic to the afferent. To address the transfer function of membrane potential across the synapse will require examination in an epithelium with a simple topology, such as in mammalian epithelia, where a single hair cell may synapse on an afferent by way of a simple calyx (Fernandez *et al.* 1988).

As in prior studies (Highstein *et al.* 2014), the failure of CNQX to block the slow afferent current argues against it being an activation of AMPA receptors (Fig. 7). The block of the current by ZD7288 indicated that the current flows through HCN channels that are known to exist in both vestibular and auditory afferents (Yi *et al.* 2010; Meredith *et al.* 2012; Kim & Holt, 2013; Liu *et al.* 2014). The block of HCN channels doubled the dominant time constant of the hair cell tail current relaxation (Fig. 7). By contrast, relief of H^+-block of the HCN channel by increased pH buffering (Fig. 8) increased ion permeation into the calyx and decreased the dominant time constant of hair cell tail relaxation by a factor of 2. In combination these results suggest that the decrease in $[K^+]_{cleft}$ is associated with K^+ efflux from the cleft, a component of which is through the postsynaptic HCN channels. One caveat with respect to the pharmacological blocking experiment is that $Na_V1.4$ channels may also be blocked by ZD7288 (Wu *et al.* 2012). However, a survey of the Na^+ channel expression in vestibular afferents has failed to reveal $Na_V1.4$ (Liu *et al.* 2016). Also arguing against the inward current being through a Na^+ conductance is that hair cell depolarization and the potassium efflux into the cleft would be associated with a decrease in $[Na^+]_{cleft}$. Such a decrease would reduce the driving force on Na^+, resulting in a net outward current, rather than the inward current observed in the afferent. A second concern is that T-type Ca^{2+} channels are known to be expressed in vestibular afferent ganglion cells (Chambard *et al.* 1999; Autret *et al.* 2005), but a reported sensitivity of these channels to ZD7288 (Felix *et al.* 2003) is unlikely to explain the block of either the hair cell induced or the standing inward current for experiments in which the afferent was held at –100 mV, a potential hyperpolarized to the threshold for T-type Ca^{2+} channel activation.

In our experiments the increase in $[K^+]_{cleft}$ near the resting potential of –70 mV has a significant contribution from the flow of K^+ through the basolateral hair cell conductances (Meredith & Rennie, 2016). The question of how the elevated $[K^+]_{cleft}$ is reduced requires considering paths for removal (Fig. 11*B*). Diffusion out of the cleft as illustrated is one such route, as is the ongoing activity of the Na^+/K^+-ATPase (Schuth *et al.* 2014). It is clear from our experiments (Fig. 5*B*) that the low-voltage-activated potassium channel remains open in the presence of elevated $[K^+]_{cleft}$, and K^+ can flow back into the hair cell for tens of milliseconds. Finally, the role of the HCN channels must be considered (Meredith *et al.* 2012; Horwitz *et al.* 2014), since the dominant time constant of the hair cell tail current was increased by ZD7288 block of the afferent HCN channels (Fig. 7*C*), and decreased by reducing their H^+-block with Hepes (Fig. 8*B*). These results demonstrate that at least some of the K^+ leaves the cleft via HCN channels as has been suggested (Meredith *et al.* 2012). The HCN channels are permeable to both Na^+ and K^+, and the $[K^+]_o$ is known to modulate Na^+ permeation, so in the absence of a detailed experimental analysis of the relative permeability of Na^+ and K^+ through these channels, it is premature to state what percentage of the inward current is carried by Na^+ and K^+ at any potential. Also of concern is that the HCN channels are expressed on both faces of the afferent. The outer face channels are bathed in perilymph at a relatively fixed $[K^+]_o$, while those on the inner face are exposed to the dynamically varying $[K^+]_{cleft}$. At the hyperpolarized potentials of our experiments, the majority of the current will be carried by Na^+, with an increased proportion carried by K^+ as $[K^+]_{cleft}$ is elevated.

Potassium feedback from postsynaptic to presynaptic cell

Our experiments demonstrated that with both cells clamped at their typical resting potentials, depolarization of either hair cell or afferent produces responses in the other that are appropriate for expected modulations of $[K^+]_{cleft}$ (Fig. 2*C* and *D*). With both cells at –70 mV the majority of the K^+ is likely to be from the hair cell since depolarization of the afferent would decrease

K^+ permeation through the inwardly rectifying HCN channels. The tail experiments (Fig. 4) are revelatory in this regard. Comparisons of the hair cell tail currents before and after an extended hair cell depolarization demonstrate that K^+ efflux from the hair cell is sufficient to raise the $[K^+]_{cleft}$. In the second set of experiments (Fig. 5), afferent depolarizations generating an outward current could also make a contribution to elevating $[K^+]_{cleft}$. The latter experiment also revealed even more significant results regarding changes in the kinetics of the gating of hair cell conductances. Regardless of any inherent voltage sensitivity of hair cell K^+ channel gating, modulation of ion concentrations in the cleft slows the kinetics of the tail currents. With the depolarization of the afferent, the hair cell tail current continues virtually unabated for the duration of the repolarization pulse (Fig. 5*A*, right series). It is well known that HCN channel voltage sensitivity and kinetics are sensitive to $[K^+]_o$ (Bader *et al.* 1982), but these results are remarkable in their demonstration that for an enveloped hair cell, the potassium-channel gating is sensitive to the $[K^+]_{cleft}$ as well.

Modes of synaptic transmission and the afferent resting potential

The EPSCs we report are larger than the values typically reported in mammalian vestibular systems (Sadeghi *et al.* 2014). The large and complex topology of the dimorphic endings is associated with afferent capacitances that may be in excess of 100 pF, but often similar to those reported previously in this species (Highstein *et al.* 2014). For quantal transmission to significantly depolarize the afferent in this context would require either large quantal events or the summation of high-frequency smaller ones. Generation of APs directly from single EPSPs varying in amplitude between 250 μV and 5 mV would require that the afferent potential be tightly regulated. Of the afferent conductances facing the synaptic cleft, depolarizing current is provided by the CNQX-sensitive glutamate receptor, augmented by a slowly-inactivating $Na_V1.5$ and the HCN conductances that provide positive feedback, tending to depolarize the afferent further. The role of negative feedback, tending to hyperpolarize the ending, would include the electrogenic effects of the Na^+/K^+-ATPase (Schuth *et al.* 2014) and a wide range of K^+ conductances (Meredith & Rennie, 2016). The driving force for these conductances will be dependent on the $[Na^+]$ and $[K^+]$ in the cleft, and as $[K^+]_{cleft}$ increases, the positive feedback (through HCN channels) increases and the negative feedback through K^+ channels decreases. Equivalent conductances on the outer face would serve equivalent functions, adding positive or negative feedback to maintain the potential, but their effects will be less dynamic since the ion concentrations in the bulk of the perilymph will remain relatively constant.

High-fidelity transmission between pre- and postsynaptic cell

HCN channels have been implicated in other sensory systems (Bader *et al.* 1979, 1982), and more generally at synaptic spines and dendritic arbours in the CNS (Lai & Jan, 2006; Paspalas *et al.* 2013). They are implicated in preserving the fidelity of synaptic inputs in auditory afferents (Yi *et al.* 2010) and along the length of apical dendrites (Lai & Jan, 2006), as well as controlling and integrating presynaptic release (He *et al.* 2014), or modulating the throughput on dendritic spines (Paspalas *et al.* 2013). In addition to these membrane effects, Na^+ flux through HCN channels is thought to modulate $[Na^+]_i$, with a resultant impact on glutamate transport into synaptic vesicles (Huang & Trussell, 2014). Such a multiplicity of roles is coherent with gating of a channel that is multiply controlled by voltage, cyclic nucleotides and ion concentration. Its distribution at restricted synaptic spaces in the nervous system, where ion concentrations change dynamically, is appropriate for a mixed conductance that is permeable to both Na^+ and K^+ ions.

We conclude from our studies of the hair cell–afferent pair that the problem of maintaining rapid and high-fidelity transmission in the presence of large conductance in both the presynaptic and postsynaptic cells is overcome by the modulatory effects of K^+ accumulation in the synaptic cleft. For the presynaptic hair cell, depolarization into the range necessary for calcium influx and synaptic vesicle fusion is accomplished in part by a shift in the equilibrium potential of the basolateral potassium conductances. For the postsynaptic afferent, the maintenance of the membrane potential necessary for the initiation of an action potential by a single quantum is achieved in large part by the sensitivity of the HCN conductance to external $[K^+]$, abetted by non-inactivating Na^+ conductances (Lysakowski *et al.* 2011; Liu *et al.* 2016) and in some preparations, a CNQX-blockable standing inward current (Sadeghi *et al.* 2014). With larger transduction currents into a hair cell, there would be higher K^+ efflux through the basolateral surface, with an associated increase in $[K^+]_{cleft}$. This would depolarize the hair cell and increase the frequency of quanta released. With the elevation in $[K^+]_{cleft}$ there would also be greater afferent depolarization, and smaller and smaller EPSPs would be sufficient to trigger APs. By the combination of these two mechanisms the rate of high-fidelity afferent discharge would be increased across a wide dynamic range. The physiological significance of large elevations of $[K^+]_{cleft}$ that depolarize afferents to potentials where inherent instability gives rise to regular, high-frequency discharge remains elusive. The majority of afferents with evenly spaced high-frequency discharge are bouton endings onto type II hair cells (Baird *et al.* 1988), rather than calyceal endings onto type I hair cells. High-frequency discharge

does highlight a possibly catastrophic behaviour, however, if ion concentrations in the synaptic cleft are not well regulated and the postsynaptic cell is tonically activated by large elevations of $[K^+]_{cleft}$.

References

Adelman WJ Jr, Palti Y & Senft JP (1973). Potassium ion accumulation in a periaxonal space and its effect on the measurement of membrane potassium ion conductance. *J Membr Biol* **13**, 387–410.

Almers W (1972). Potassium conductance changes in skeletal muscle and the potassium concentration in the transverse tubules. *J Physiol* **225**, 33–56.

Araque A, Parpura V, Sanzgiri RP & Haydon PG (1999). Tripartite synapses: glia, the unacknowledged partner. *Trends Neurosci* **22**, 208–215.

Attwell D, Cohen I & Eisner D (1979). Membrane potential and ion concentration stability conditions for a cell with a restricted extracellular space. *Proc R Soc Lond B Biol Sci* **206**, 145–161.

Attwell D & Iles JF (1979). Synaptic transmission: ion concentration changes in the synaptic cleft. *Proc R Soc Lond B Biol Sci* **206**, 115–131.

Autret L, Mechaly I, Scamps F, Valmier J, Lory P & Desmadryl G (2005). The involvement of Cav3.2/α1H T-type calcium channels in excitability of mouse embryonic primary vestibular neurones. *J Physiol* **567**, 67–78.

Bader CR, Bertrand D & Schwartz EA (1982). Voltage-activated and calcium-activated currents studied in solitary rod inner segments from the salamander retina. *J Physiol* **331**, 253–284.

Bader CR, Macleish PR & Schwartz EA (1979). A voltage-clamp study of the light response in solitary rods of the tiger salamander. *J Physiol* **296**, 1–26.

Baird RA, Desmadryl G, Fernandez C & Goldberg JM (1988). The vestibular nerve of the chinchilla. II. Relation between afferent response properties and peripheral innervation patterns in the semicircular canals. *J Neurophysiol* **60**, 182–203.

Bao H, Wong WH, Goldberg JM & Eatock RA (2003). Voltage-gated calcium channel currents in type I and type II hair cells isolated from the rat crista. *J Neurophysiol* **90**, 155–164.

Baylor DA & Fettiplace R (1976). Transmission of signals from photoreceptors to ganglion cells in the eye of the turtle. *Cold Spring Harb Symp Quant Biol* **40**, 529–536.

Borst JG & Soria van Hoeve J (2012). The calyx of Held synapse: from model synapse to auditory relay. *Annu Rev Physiol* **74**, 199–224.

Brichta AM & Goldberg JM (2000*a*). Morphological identification of physiologically characterized afferents innervating the turtle posterior crista. *J Neurophysiol* **83**, 1202–1223.

Brichta AM & Goldberg JM (2000*b*). Responses to efferent activation and excitatory response-intensity relations of turtle posterior-crista afferents. *J Neurophysiol* **83**, 1224–1242.

Chabbert C, Chambard JM, Valmier J, Sans A & Desmadryl G (2001). Hyperpolarization-activated (I_h) current in mouse vestibular primary neurons. *Neuroreport* **12**, 2701–2704.

Chambard JM, Chabbert C, Sans A & Desmadryl G (1999). Developmental changes in low and high voltage-activated calcium currents in acutely isolated mouse vestibular neurons. *J Physiol* **518**, 141–149.

Chatlani S (2011). Whole-cell recordings from vestibular calyx endings of the turtle posterior crista. PhD Thesis, University of Chicago, Chicago.

Chen W-Y (1995). The properties and functions of a low-voltage activated K1 current in type I hair cells of rat semicircular canal organs. PhD Thesis, University of Rochester, Rochester, NY.

Cho S & von Gersdorff H (2014). Proton-mediated block of Ca^{2+} channels during multivesicular release regulates short-term plasticity at an auditory hair cell synapse. *J Neurosci* **34**, 15877–15887.

Church J, Baxter KA & McLarnon JG (1998). pH modulation of Ca^{2+} responses and a Ca^{2+}-dependent K^+ channel in cultured rat hippocampal neurones. *J Physiol* **511**, 119–132.

Cichy A, Ackels T, Tsitoura C, Kahan A, Gronloh N, Sochtig M, Engelhardt CH, Ben-Shaul Y, Muller F, Spehr J & Spehr M (2015). Extracellular pH regulates excitability of vomeronasal sensory neurons. *J Neurosci* **35**, 4025–4039.

Cohen I, Daut J & Noble D (1976). The effects of potassium and temperature on the pace-maker current, iK2, in Purkinje fibres. *J Physiol* **260**, 55–74.

Contini D (2011). Intercellular K^+ accumulation drives Type I hair cells into the activation range of voltage-gated Ca channels. PhD Thesis, University of Pavia, Pavia, Italy.

Contini D, Zampini V, Tavazzani E, Magistretti J, Russo G, Prigioni I & Masetto S (2012). Intercellular K^+ accumulation depolarizes Type I vestibular hair cells and their associated afferent nerve calyx. *Neuroscience* **227**, 232–246.

Dalet A, Bonsacquet J, Gaboyard-Niay S, Calin-Jageman I, Chidavaenzi RL, Venteo S, Desmadryl G, Goldberg JM, Lysakowski A & Chabbert C (2012). Glutamate transporters EAAT4 and EAAT5 are expressed in vestibular hair cells and calyx endings. *PLoS One* **7**, e46261.

DeRosier DJ & Tilney LG (1989). The structure of the cuticular plate, an in vivo actin gel. *J Cell Biol* **109**, 2853–2867.

DeVries SH (2001). Exocytosed protons feedback to suppress the Ca^{2+} current in mammalian cone photoreceptors. *Neuron* **32**, 1107–1117.

Dhawan R, Mann SE, Meredith FL & Rennie KJ (2010). K^+ currents in isolated vestibular afferent calyx terminals. *J Assoc Res Otolaryngol* **11**, 463–476.

Du J, Reznikov LR, Price MP, Zha XM, Lu Y, Moninger TO, Wemmie JA & Welsh MJ (2014). Protons are a neurotransmitter that regulates synaptic plasticity in the lateral amygdala. *Proc Natl Acad Sci USA* **111**, 8961–8966.

Eatock RA & Songer JE (2011). Vestibular hair cells and afferents: two channels for head motion signals. *Annu Rev Neurosci* **34**, 501–534.

Felix R, Sandoval A, Sanchez D, Gomora JC, De la Vega-Beltran JL, Trevino CL & Darszon A (2003). ZD7288 inhibits low-threshold Ca^{2+} channel activity and regulates sperm function. *Biochem Biophys Res Commun* **311**, 187–192.

Fernandez C, Baird RA & Goldberg JM (1988). The vestibular nerve of the chinchilla. I. Peripheral innervation patterns in the horizontal and superior semicircular canals. *J Neurophysiol* **60**, 167–181.

Fettiplace R & Crawford AC (1978). The coding of sound pressure and frequency in cochlear hair cells of the terrapin. *Proc R Soc Lond B Biol Sci* **203**, 209–218.

Forsythe ID (1994). Direct patch recording from identified presynaptic terminals mediating glutamatergic EPSCs in the rat CNS, in vitro. *J Physiol* **479**, 381–387.

Frankenhaeuser B & Hodgkin AL (1956). The after-effects of impulses in the giant nerve fibres of *Loligo*. *J Physiol* **131**, 341–376.

Fuchs PA & Glowatzki E (2015). Synaptic studies inform the functional diversity of cochlear afferents. *Hear Res* **330**, 18–25.

Gabbiani F & Koch C (2003). Priciples of spike train analysis. In *Methods in Neuronal Modeling: From Ions to Networks*, 2nd edn, ed. Koch C & Segev I, pp. 313–360. MIT Press, Cambridge, MA, USA.

Gasparini S & DiFrancesco D (1997). Action of the hyperpolarization-activated current (I_h) blocker ZD 7288 in hippocampal CA1 neurons. *Pflugers Arch* **435**, 99–106.

Glowatzki E & Fuchs PA (2002). Transmitter release at the hair cell ribbon synapse. *Nat Neurosci* **5**, 147–154.

Goldberg JM (1996*a*). Theoretical analysis of intercellular communication between the vestibular type I hair cell and its calyx ending. *J Neurophysiol* **76**, 1942–1957.

Goldberg JM (1996*b*). Transmission between the type I hair cell and its calyx ending. *Ann NY Acad Sci* **781**, 474–488.

Goldberg JM & Holt JC (2013). Discharge regularity in the turtle posterior crista: comparisons between experiment and theory. *J Neurophysiol* **110**, 2830–2848.

Goldberg JM, Lysakowski A & Fernandez C (1990). Morphophysiological and ultrastructural studies in the mammalian cristae ampullares. *Hear Res* **49**, 89–102.

Goodman MB & Art JJ (1996). Positive feedback by a potassium-selective inward rectifier enhances tuning in vertebrate hair cells. *Biophys J* **71**, 430–442.

Haydon PG & Nedergaard M (2015). How do astrocytes participate in neural plasticity? *Cold Spring Harb Perspect Biol* **7**, a020438.

He C, Chen F, Li B & Hu Z (2014). Neurophysiology of HCN channels: from cellular functions to multiple regulations. *Prog Neurobiol* **112**, 1–23.

Highstein SM, Holstein GR, Mann MA & Rabbitt RD (2014). Evidence that protons act as neurotransmitters at vestibular hair cell-calyx afferent synapses. *Proc Natl Acad Sci USA* **111**, 5421–5426.

Highstein SM, Mann MA, Holstein GR & Rabbitt RD (2015). The quantal component of synaptic transmission from sensory hair cells to the vestibular calyx. *J Neurophysiol* **113**, 3827–3835.

Holt JC, Chatlani S, Lysakowski A & Goldberg JM (2007). Quantal and nonquantal transmission in calyx-bearing fibers of the turtle posterior crista. *J Neurophysiol* **98**, 1083–1101.

Horwitz GC, Risner-Janiczek JR & Holt JR (2014). Mechanotransduction and hyperpolarization-activated currents contribute to spontaneous activity in mouse vestibular ganglion neurons. *J Gen Physiol* **143**, 481–497.

Huang H & Trussell LO (2014). Presynaptic HCN channels regulate vesicular glutamate transport. *Neuron* **84**, 340–346.

Karunanithi S, Marin L, Wong K & Atwood HL (2002). Quantal size and variation determined by vesicle size in normal and mutant Drosophila glutamatergic synapses. *J Neurosci* **22**, 10267–10276.

Katz B (1969). *The Release of Neural Transmitter Substances*. The Sherrington Lectures, vol. 10. Liverpool University Press, Liverpool.

Katz B & Miledi R (1982). An endplate potential due to potassium released by the motor nerve impulse. *Proc R Soc Lond B Biol Sci* **216**, 497–507.

Katz B & Schmitt OH (1940). Electric interaction between two adjacent nerve fibres. *J Physiol* **97**, 471–488.

Kim YH & Holt JR (2013). Functional contributions of HCN channels in the primary auditory neurons of the mouse inner ear. *J Gen Physiol* **142**, 207–223.

Kreple CJ, Lu Y, Taugher RJ, Schwager-Gutman AL, Du J, Stump M, Wang Y, Ghobbeh A, Fan R, Cosme CV, Sowers LP, Welsh MJ, Radley JJ, LaLumiere RT & Wemmie JA (2014). Acid-sensing ion channels contribute to synaptic transmission and inhibit cocaine-evoked plasticity. *Nat Neurosci* **17**, 1083–1091.

Krishtal OA & Pidoplichko VI (1981*a*). A receptor for protons in the membrane of sensory neurons may participate in nociception. *Neuroscience* **6**, 2599–2601.

Krishtal OA & Pidoplichko VI (1981*b*). A "receptor" for protons in small neurons of trigeminal ganglia: possible role in nociception. *Neurosci Lett* **24**, 243–246.

Lai HC & Jan LY (2006). The distribution and targeting of neuronal voltage-gated ion channels. *Nat Rev Neurosci* **7**, 548–562.

Leao KE, Leao RN & Walmsley B (2011). Modulation of dendritic synaptic processing in the lateral superior olive by hyperpolarization-activated currents. *Eur J Neurosci* **33**, 1462–1470.

Lim R, Kindig AE, Donne SW, Callister RJ & Brichta AM (2011). Potassium accumulation between type I hair cells and calyx terminals in mouse crista. *Exp Brain Res* **210**, 607–621.

Lisman JE, Raghavachari S & Tsien RW (2007). The sequence of events that underlie quantal transmission at central glutamatergic synapses. *Nat Rev Neurosci* **8**, 597–609.

Liu Q, Manis PB & Davis RL (2014). I_h and HCN channels in murine spiral ganglion neurons: tonotopic variation, local heterogeneity, and kinetic model. *J Assoc Res Otolaryngol* **15**, 585–599.

Liu XP, Wooltorton J, Gaboyard-Niay S, Yang FC, Lysakowski A & Eatock RA (2016). Sodium channel diversity in the vestibular ganglion: Tetrodotoxin-sensitive, Nav1.5 and Nav1.8 currents. *J Neurophysiol* 115, 2536–2555.

Llinas R, Steinberg IZ & Walton K (1976). Presynaptic calcium currents and their relation to synaptic transmission: voltage clamp study in squid giant synapse and theoretical model for the calcium gate. *Proc Natl Acad Sci USA* **73**, 2918–2922.

Lysakowski A, Gaboyard-Niay S, Calin-Jageman I, Chatlani S, Price SD & Eatock RA (2011). Molecular microdomains in a sensory terminal, the vestibular calyx ending. *J Neurosci* **31**, 10101–10114.

Lysakowski A & Goldberg J (2004). Morphophysiology of the vestibular periphery. In *The Vestibular System*, ed Highstein SM, Popper A & Fay RR, pp. 57–152. Springer, New York.
Meredith FL, Benke TA & Rennie KJ (2012). Hyperpolarization-activated current (Ih) in vestibular calyx terminals: characterization and role in shaping postsynaptic events. *J Assoc Res Otolaryngol* **13**, 745–758.
Meredith FL & Rennie KJ (2016). Channeling your inner ear potassium: K channels in vestibular hair cells. *Hear Res* 338, 40–51.
Molecular Devices (2008). *The Axon Guide – A Guide to Electrophysiology and Biophysics Laboratory Techniques*. MDS Analytical Technologies, Sunnyvale, CA, USA.
Moroni A, Barbuti A, Altomare C, Viscomi C, Morgan J, Baruscotti M & DiFrancesco D (2000). Kinetic and ionic properties of the human HCN2 pacemaker channel. *Pflugers Arch* **439**, 618–626.
Munsch T & Pape HC (1999). Modulation of the hyperpolarization-activated cation current of rat thalamic relay neurones by intracellular pH. *J Physiol* **519**, 493–504.
Nedergaard M (1994). Direct signaling from astrocytes to neurons in cultures of mammalian brain cells. *Science* **263**, 1768–1771.
Nicoll RA (1979). Dorsal root potentials and changes in extracellular potassium in the spinal cord of the frog. *J Physiol* **290**, 113–127.
Ohmori H (1985). Mechano-electrical transduction currents in isolated vestibular hair cells of the chick. *J Physiol* **359**, 189–217.
Parpura V, Basarsky TA, Liu F, Jeftinija K, Jeftinija S & Haydon PG (1994). Glutamate-mediated astrocyte–neuron signalling. *Nature* **369**, 744–747.
Paspalas CD, Wang M & Arnsten AF (2013). Constellation of HCN channels and cAMP regulating proteins in dendritic spines of the primate prefrontal cortex: potential substrate for working memory deficits in schizophrenia. *Cereb Cortex* **23**, 1643–1654.
Photowala H, Blackmer T, Schwartz E, Hamm HE & Alford S (2006). G protein $\beta\gamma$-subunits activated by serotonin mediate presynaptic inhibition by regulating vesicle fusion properties. *Proc Natl Acad Sci USA* **103**, 4281–4286.
Press WH, Teukolsky SA, Vetterline WT & Flannery BP (1992). *Numerical Recipes in C*. Cambridge University Press, Cambridge, UK.
Rennie KJ & Ashmore JF (1991). Ionic currents in isolated vestibular hair cells from the guinea-pig crista ampullaris. *Hearing Res* **51**, 279–292.
Rennie KJ & Correia MJ (1994). Potassium currents in mammalian and avain isolated type I semicircular canal hair cells. *J Neurophysiol* **71**, 317–329.
Rennie KJ & Correia MJ (2000). Effects of cationic substitutions on delayed rectifier current in type I vestibular hair cells. *J Membr Biol* **173**, 139–148.
Rennie KJ & Streeter MA (2006). Voltage-dependent currents in isolated vestibular afferent calyx terminals. *J Neurophysiol* **95**, 26–32.
Rusch A, Lysakowski A & Eatock RA (1998). Postnatal development of type I and type II hair cells in the mouse utricle: acquisition of voltage-gated conductances and differentiated morphology. *J Neurosci* **18**, 7487–7501.
Rutherford MA, Chapochnikov NM & Moser T (2012). Spike encoding of neurotransmitter release timing by spiral ganglion neurons of the cochlea. *J Neurosci* **32**, 4773–4789.
Sadeghi SG, Pyott SJ, Yu Z & Glowatzki E (2014). Glutamatergic signaling at the vestibular hair cell calyx synapse. *J Neurosci* **34**, 14536–14550.
Schessel DA & Highstein SM (1981). Is transmission between the vestibular type I hair cell and its primary afferent chemical? *Ann NY Acad Sci* **374**, 210–214.
Schneggenburger R & Forsythe ID (2006). The calyx of Held. *Cell Tissue Res* **326**, 311–337.
Schuth O, McLean WJ, Eatock RA & Pyott SJ (2014). Distribution of Na,K-ATPase α subunits in rat vestibular sensory epithelia. *J Assoc Res Otolaryngol* **15**, 739–754.
Schweizer FE, Savin D, Luu C, Sultemeier DR & Hoffman LF (2009). Distribution of high-conductance calcium-activated potassium channels in rat vestibular epithelia. *J Comp Neurol* **517**, 134–145.
Shin KS, Rothberg BS & Yellen G (2001). Blocker state dependence and trapping in hyperpolarization-activated cation channels: evidence for an intracellular activation gate. *J Gen Physiol* **117**, 91–101.
Stadler H & Tsukita S (1984). Synaptic vesicles contain an ATP-dependent proton pump and show 'knob-like' protrusions on their surface. *EMBO J* **3**, 3333–3337.
Sterio DC (1984). The unbiased estimation of number and sizes of arbitrary particles using the disector. *J Microsc* **134**, 127–136.
Vaaga CE, Borisovska M & Westbrook GL (2014). Dual-transmitter neurons: functional implications of co-release and co-transmission. *Curr Opin Neurobiol* **29**, 25–32.
Wersäll J (1956). Studies on the structure and innervation of the sensory epithelium of the cristae ampullares in the guinea pig. *Acta Otolaryngol Suppl* 126, 1–85.
Wu X, Liao L, Liu X, Luo F, Yang T & Li C (2012). Is ZD7288 a selective blocker of hyperpolarization-activated cyclic nucleotide-gated channel currents? *Channels (Austin)* **6**, 438–442.
Yi E, Roux I & Glowatzki E (2010). Dendritic HCN channels shape excitatory postsynaptic potentials at the inner hair cell afferent synapse in the mammalian cochlea. *J Neurophysiol* **103**, 2532–2543.
Zong X, Stieber J, Ludwig A, Hofmann F & Biel M (2001). A single histidine residue determines the pH sensitivity of the pacemaker channel HCN2. *J Biol Chem* **276**, 6313–6319.

Additional information

Competing interests

The authors have no competing interests.

Author contributions

D.C. was involved in the conception and design of the study, collection and analysis of data, and drafting the manuscript.

S.D.P. was involved in the design of the study, and collection, assembly and interpretation of the microscopic data. J.J.A. contributed to the conception and design of the study, collection, assembly, analysis and interpretation of the data, and manuscript writing. The work was performed in the laboratory of J.J.A. and used the common core microscopy facilities, financial, and administrative support of the Department of Anatomy & Cell Biology. All authors have approved the final version of the manuscript, agree to be accountable for all aspects of the work, and qualify for authorship. All those who qualify for authorship are listed.

Funding

This work was funded by the NIH: National Institute on Deafness and Other Communication Disorders, grant number R01 DC002058.

Acknowledgements

We thank Dr Gay Holstein for the loan of equipment. We also thank Drs Mark Brodie, Robert Fettiplace, Miriam Goodman, Gay Holstein and Eric Schwartz for useful discussions and comments on prior versions of the manuscript.

Translational perspective

We demonstrate that the K^+ concentration is higher in the synaptic cleft than the bulk extracellular solution and that this serves as a modulator of synaptic transmission in the femtolitre space of the synapse. The elevated K^+ concentration in the cleft is sufficient to depolarize the presynaptic hair cell to potentials necessary for the quantal release of transmitter. It also generates an inward current through hyperpolarization-activated cyclic nucleotide-gated (HCN) channels, and these channels hold the postsynaptic neuron close to the threshold for action potential generation. As a result, the elevated synaptic K^+ concentrations enable a single vesicle (quantum) released presynaptically to trigger a single action potential in the postsynaptic neuron, ensuring that the statistics of postsynaptic activity match the statistics of vesicle release, thereby maintaining high-frequency, high-fidelity information transfer. However, we have also demonstrated that the postsynaptic cell can be tonically activated by large elevations of $[K^+]_{cleft}$. This opens the possibility that a pharmacological block of HCN channels in addition to glutamate receptors may be an efficacious treatment for certain forms of epilepsy. HCN channels are common in the CNS where they are present not only in dendrites in the cerebral cortex, but also at synapses in hippocampus, midbrain, cerebellum and brainstem. Modulation of this channel by synaptic K^+ ions is likely to be a general feature of central synaptic transmission. These results further suggest that at dendritic spines and other synapses with restricted extracellular spaces, the roles of elements traditionally characterized as pre- and postsynaptic must be critically re-evaluated.